Theoretical Study of the Effect of (001) TiO_2 Anatase Support on V_2O_5

Konstantinos Alexopoulos,[†] Pawel Hejduk,[‡] Malgorzata Witko,[‡] Marie-Francoise Reyniers,*[,†] and Guy B. Marin[†]

Laboratory for Chemical Technology, Ghent University, Krijgslaan 281 (S5), B-9000 Ghent, Belgium, and Institute of Catalysis and Surface Chemistry, Polish Academy of Sciences, Niezapominajek 8, 30239 Cracow, Poland

Received: November 10, 2009; Revised Manuscript Received: January 7, 2010

The effect of (001) TiO_2 anatase support on the electronic and catalytic properties of a V_2O_5 monolayer is analyzed using density functional theory (DFT). The catalyst is represented by both clusters and periodic slabs. Using two experimentally relevant models of monolayer V_2O_5/TiO_2 (anatase) catalyst, both weak and strong interactions between a V_2O_5 monolayer and the TiO_2 support have been investigated. In the first model, where a crystallographic (001) V_2O_5 layer is placed on top of the (001) TiO_2 support, the weak interaction between vanadia and titania does not result in a major reconstruction of the active phase. Nevertheless, the changes in the electronic properties of the system are evident. The deposition of the vanadia monolayer on the titania substrate results in charge redistribution, enhancing the Lewis acidity of vanadium and the chemical hardness above the vanadyl oxygen, and in a shift of the Fermi level to lower binding energies accompanied by a reduction in the band gap. In the second model, where the (001) titania anatase structure is extended with a VO_2 film terminated by half a monolayer of vanadyl oxygen, apart from a similar electronic effect, the strong interaction of the vanadia phase with the titania support resulting from a high order of epitaxy has an important effect on the structure of the active phase. Atomic hydrogen adsorption is most favorable on the vanadyl oxygen of all the investigated surfaces, while the adsorption energy on this site increases by ~10 kJ/mol due to the weak interaction between vanadia and titania and is further increased by ~50 kJ/mol as a stronger interaction between the two phases is achieved, all in agreement with the increase in the negative electrostatic potential above the vanadyl site. The observed trends in the reactivity of the oxygen sites in H adsorption for the different catalyst models are successfully explained in terms of a frontier orbital analysis.

Introduction

Transition metal oxides are widely used as catalysts for the oxidation of hydrocarbons. Especially vanadium oxide based catalysts are among the most active for the oxidation of both aliphatic and aromatic hydrocarbons. An important example of such a catalyst is V_2O_5/TiO_2 (anatase), which is used in industry as an effective catalyst for the production of phthalic anhydride from *o*-xylene.[1,2] For the anatase support, although the (101) surface is thermodynamically more stable, the (100) and (001) faces are found in the industrial TiO_2 powders.[3] Earlier experimental studies indicate that this catalytic system is of high performance when it consists of a monolayer of V_2O_5 upon a TiO_2 (anatase) substrate, showing activity and selectivity not observed in the unsupported V_2O_5 or TiO_2 anatase.[2,4] The enhanced catalytic performance can be attributed to a synergetic effect between the active phase and the support. In order to unravel the role of the TiO_2 support on a V_2O_5 monolayer catalyst, ab initio methods can help to provide a better understanding of the relation between structure and reactivity.

Several theoretical models have been proposed for describing the V_2O_5/TiO_2 anatase catalyst at different vanadium loadings. Avdeev and Zhidomirov[5] used small cluster models consisting of monovanadate and divanadate species to model the active centers of the V_2O_5/TiO_2 catalyst. They found that TiO_2 forms strong bonds with the monomeric and dimeric VO_x groups. Kachurovskaya et al.[6] constructed cluster models of the VO_x/TiO_2 catalyst based on embedding vanadium ions in the anatase support. This is the so-called substitution model, as it consists of replacing a surface Ti atom by a V or VOH unit. Their results indicated an increased acidity of the VO_x/TiO_2 catalyst system as compared to pure V_2O_5. Additionally they concluded that including a second titania layer is essential for the modeling of the anatase support. Besides cluster models, the periodic approach has also been used to model the V_2O_5/TiO_2 catalyst. This approach is mostly useful for investigating medium and high coverages of vanadia on titania. In order to model coverages of vanadia below the monolayer, Calatayud and Minot[3] have constructed periodic slabs consisting of monomeric and dimeric vanadia species deposited on titania anatase, which is an example of the so-called addition model. Moreover, Grybos and Witko[7] used different monomers with the general formula of VO_xH_y to construct vanadium oxide monolayers on a TiO_2 anatase slab. In both of these studies, the vanadia species are anchored to the anatase support by strong interactions.

In general, the interaction of the support with the active phase of the catalyst can be either strong or weak, depending on whether the presence of the support modifies significantly the structure of the active phase or not.[7] Devriendt et al.[8] put several models[9−12] of the V_2O_5/TiO_2 anatase catalyst to the test using single scattering cluster simulations in conjunction with X-ray photoelectron diffraction (XPD) measurements. Either these models consisted of mono-oxo[9] (V═O) or dioxo[10] (O═V═O) vanadyl groups centered above four or two anatase surface

* Corresponding author: tel, +32 9 264 5677; fax, +32 9 264 5824; e-mail, MarieFrancoise.Reyniers@ugent.be.
[†] Laboratory for Chemical Technology, Ghent University.
[‡] Institute of Catalysis and Surface Chemistry, Polish Academy of Sciences.

10.1021/jp910685z

oxygen atoms, respectively, or they[11,12] assumed that the vanadia monolayer has a structure similar to the crystalline V_2O_5. Although the authors[8] concluded that the model resembling a flattened V_2O_5 (001) layer[11] provided the best fit, this model needs to be refined in order to eliminate the lattice misfit strain at the interface. However, according to the same authors,[8] the relaxation of the V_2O_5 (001) monolayer by means of simulations based on force fields[12] was considered to be too strong, and it was suggested that a more bulklike V_2O_5 structure would be able to explain the experimental XPD patterns. In agreement with this, X-ray absorption spectroscopy (XAS) measurements[13] yielded no structural differences between the fully oxidized supported vanadium oxide and bulk crystalline V_2O_5. On the other hand, results obtained for V_2O_5/TiO_2 anatase by X-ray photoelectron spectroscopy (XPS), UV photoelectron spectroscopy, reflection high energy electron diffraction, and low energy electron diffraction measurements[14] and periodic DFT calculations[15] pointed toward an epitaxial monolayer with a V_2O_5 stoichiometry. In addition, periodic DFT calculations for thin vanadia films on Al_2O_3 support[16] yielded similar conclusions, since a pseudomorphic epitaxial V_2O_3 layer with oxygen adsorption oxidizing the outermost V to 5+ is favored. Thus, the composition of the surface layer is V_2O_5, but the coordination of vanadium is different from that in the crystallographic V_2O_5 (001) layer.

In an attempt to clarify the nature of the interaction between the support and the active phase, two supported models of a V_2O_5 monolayer have been proposed in this study and are confronted to results available in literature. In the first model, where a weak interaction between the support and the active phase is assumed, a crystallographic V_2O_5 (001) layer is placed on top of the (001) TiO_2 anatase support, which is allowed due to the small lattice misfit between the two phases.[12] In the second model, where a strong interaction between the two phases is assumed, the (001) titania anatase structure is extended with a VO_2 film terminated by half of monolayer of vanadyl oxygen, thus creating a vanadia monolayer that does not resemble the structure of bulk V_2O_5 but has the fully oxidized V_2O_5 stoichiometry.[14] Moreover, for both models all the possible orientations of the active V_2O_5 phase on the support have been considered. Apart from the supported catalyst system, models have also been constructed for the most stable (001) V_2O_5 surface of the unsupported V_2O_5 catalyst and for the (001) TiO_2 anatase support surface typically found in the industrial TiO_2 powders. In order to investigate the influence of the support on the vanadia monolayer, a comparison of the electronic properties, e.g., atomic charges, bond orders, electrostatic potential, and density of states, between the supported and the unsupported catalytic systems is made. Additionally, the adsorption of atomic hydrogen is used to probe the reactivity of the different active sites that exist on the vanadia surface.

Methodology

Computational Details. ***Periodic Calculations.*** Spin-polarized periodic DFT calculations have been carried out with the Vienna Ab Initio Simulation Package (VASP) using plane wave basis sets.[17,18] A plane-wave energy cutoff of 400 eV has been used in all cases. The projector augmented wave method of Blöchl[19] in the implementation of Kresse and Joubert[20] has been chosen to describe the electron−ion interaction. To account for the nonlocality in the exchange correlation functional, the generalized gradient approximation (GGA) according to Perdew, Burke, and Ernzerhof (PBE) has been used.[21] The catalyst is represented as an infinite system with periodic symmetry.[22] A conjugate-gradient algorithm has been utilized to relax the atoms into their instantaneous ground state, assuming that convergence is achieved when the forces are below 0.05 eV/Å. The Monkhorst−Pack division scheme[23] has been chosen to generate a set of *k*-points within the Brillouin zone. To improve the convergence with respect to the number of *k*-points without affecting the accuracy of the calculation, a Gaussian smearing[18,24] of 0.05 eV has been applied. Convergence tests regarding the number of *k*-points, the size of the surface slabs, and the thickness of the vacuum layers have been carried out to ensure an accurate description of the catalytic system. A $2 \times 6 \times 6$ and a $6 \times 6 \times 2$ *k*-point mesh was found to be adequate for the bulk V_2O_5 and TiO_2 anatase, respectively, yielding cohesive energies that are converged within 1 meV. Accordingly, for the (1×1) primitive surface cell of (001) V_2O_5 and for the (3×1) supercell of (001) TiO_2 a $2 \times 6 \times 1$ *k*-point mesh was applied, while a $3 \times 3 \times 1$ *k*-point mesh was used for the (2×2) supercell of (001) TiO_2. A vacuum gap of ~11 Å was found sufficient to separate subsequent slabs, yielding surface energies that are converged within 0.001 J/m^2. For the surface calculations, no symmetry was used and a dipole correction was included. In all cases, the vanadia monolayer is fully relaxed, while the atoms of the titania support are kept fixed to their bulk positions. As a second optimization step, some calculations have also been performed allowing the topmost layer of the titania support to relax together with the vanadia monolayer, thus being able to determine the effect of this extra relaxation on the structure and energetics of the supported system. For the unsupported vanadia, surface energies are calculated as

$$\Delta E_{\text{surf}} = \frac{1}{2A}(E_{\text{surf}} - E_{\text{bulk}}) \quad (1)$$

where A is the surface area, E_{surf} is the energy of the V_2O_5 surface unit cell, and E_{bulk} is the energy of the V_2O_5 bulk unit cell. For the supported vanadia monolayer, surface formation energies[25] are calculated as

$$\Delta E_{\text{f(surf)}} = \frac{1}{A}[E_{V_2O_5/TiO_2(\text{surf})} - E_{V_2O_5(\text{bulk})} - E_{TiO_2(001)}] \quad (2)$$

where A is the surface area, $E_{V_2O_5/TiO_2(\text{surf})}$ is the energy of the surface cell of the supported vanadia on titania system, $E_{TiO_2(001)}$ is the energy of the (001) TiO_2 anatase surface cell, and $E_{V_2O_5(\text{bulk})}$ is the energy of the V_2O_5 bulk unit cell. In addition, adsorption energies of atomic hydrogen on the surface are calculated as follows using supercells having surface area of ~80 Å^2

$$\Delta E_{\text{ads}} = E_{\text{vanadia/H}} - (E_{\text{vanadia}} + E_{\text{H}}) \quad (3)$$

where $E_{\text{vanadia/H}}$ refers to the energy of the hydroxylated unsupported/supported vanadia surface, E_{vanadia} refers to the energy of the clean unsupported/supported vanadia surface, and E_{H} refers to the energy of an isolated hydrogen atom. Positive values of ΔE_{ads} indicate endothermic processes, while negative values indicate exothermic processes.

After geometry optimization of the periodic models, band structure calculations have been performed using VASP in order to map the electronic structure of the investigated systems. The bands are plotted along directions connecting high symmetry points inside the irreducible part of the Brillouin zone, which in all investigated cases is orthorhombic (Figure 1). These graphs reveal the energy dispersion of each band along different symmetry lines, thus characterizing the anisotropy of the material. In order to have a clear separation between the occupied and unoccupied bands, the energy scale of these graphs is relative to the Fermi level of each system. Next to that, the total spin-up and spin-down density of states (DOS) are readily

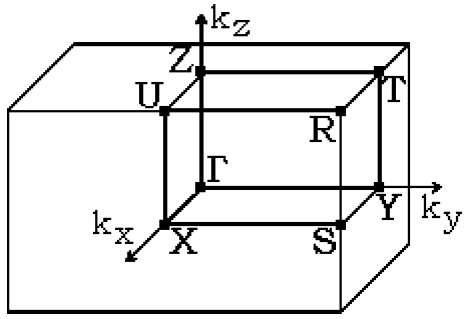

Figure 1. First Brillouin zone of the orthorhombic lattice and its high symmetry points.

obtained from the band structure calculations and can be used to observe whether there are any unpaired electron states. However, because band structures and their *k*-space integrals, i.e., DOS, do not contain any information about the localization of the electronic states in real space or to which atom these states belong to, local or partial DOS (p-DOS) are also calculated by projecting the plane waves onto specific atomic orbitals. Moreover, to obtain a measure of the atomic charges for each periodic model, a Bader analysis[26] is performed as implemented by Henkelman et al.,[27] using the charge density calculated by VASP. In this implementation the core charges are also included in the partitioning of the charge density, thus increasing the accuracy of the method. In addition, to have a clear-cut view of the charge redistribution induced by the bonding between vanadia and titania, a charge density difference is calculated as

$$\Delta\rho = \rho_{V_2O_5/TiO_2} - \rho_{V_2O_5} - \rho_{TiO_2} \quad (4)$$

where ρ is the charge density calculated by VASP for each surface model. Finally, the electrostatic potential for the investigated surface models is also calculated using VASP. According to literature,[28] this property, which describes the interaction energy of a system with a positive unit charge (proton), can be used as a DFT based reactivity indicator probing the hard regions of the surface. More specifically, the region with the most negative value of the electrostatic potential is most favorable to undergo a hard electrophilic attack.

Cluster Calculations. According to Sauer and Dobler,[29] GGA functionals like PBE typically used in plane wave calculations may yield electronic structures that are too delocalized and the use of hybrid functionals has been recommended in such cases. Therefore, in order to provide a more localized picture around the region where the bonding between vanadia and titania takes place, density functional theory (DFT) cluster calculations have been performed with Turbomole,[30−32] using the hybrid PBE0 functional[21] and all-electron triple-ζ plus polarization basis sets[33] (TZVP) on all atoms. An advantage of this approach is that one can use the whole spectrum of quantum-chemical methods developed for small molecules with relatively minor modifications.[34] The catalytic system is represented as clusters cut out of the catalyst's surface with the dangling bonds at the cluster periphery saturated by hydrogen atoms.[22] Geometry optimizations were done with Turbomole using the default convergence criteria, i.e., 10^{-3} atomic units (0.05 eV/Å) for the maximum norm of the Cartesian gradient, while single point calculations were also performed with Gaussian03[35] at the PBE0/TZVP level. The hydrogen-terminating atoms and the atoms belonging to the titania support were kept fixed during geometry optimization. In all cases, cluster size convergence tests have been carried out to ensure an accurate description of the investigated systems. For the cases where a vanadia cluster representing the (001) V_2O_5 surface is placed on top of a titania cluster representing the (001) TiO_2 anatase support, the energy change involved in this process is expressed as follows

$$\Delta E_{f(cluster)} = E(V_{10}O_{31}H_{12}/Ti_xO_yH_{2y-4x}) - E(V_{10}O_{31}H_{12}) - E(Ti_xO_yH_{2y-4x}) \quad (5)$$

while the electron density difference is calculated according to eq 4, using the electron density calculated by Turbomole for each cluster model.

Atomic charges for the cluster models have been calculated with Turbomole using a Mulliken population analysis[36] and a modified Roby−Davidson population analysis based on occupation numbers[37] and with Gaussian03 using a Bader analysis based on the same implementation[26,27] as for the periodic models. Next to the atomic charges, Wiberg bond orders[38] have been calculated with Gaussian03 as total per atom in order to probe the covalent nature of the investigated systems. For all the aforementioned population analyses, the values are always taken from the atoms located at the center of the cluster, as they are the most representative ones. In addition, the electronic structure of the cluster models is analyzed with Gaussian03 using electrostatic potential maps, partial densities of states projected on certain representative atoms (p-DOS), and crystal orbital overlap populations[39] projected on certain representative bonds (p-COOP). Due to the discrete orbital energy levels of the cluster, a Gaussian broadening of 0.5 eV is applied for the construction of p-DOS and p-COOP curves.

Models. ***Bulk V_2O_5 and TiO_2 Anatase.*** Bulk V_2O_5 forms a layer-type orthorhombic lattice with space group *Pmmn* (D_{2h}^{13}) and experimental lattice constants $a = 11.512$ Å, $b = 3.564$ Å, and $c = 4.368$ Å.[40] Its unit cell, V_4O_{10}, comprises two formula units. In the crystal structure (Figure 2), the layers are stacked in such a way that distorted VO_6 octahedra are formed with V−O bond distances varying between rather small (1.58 Å) and quite large values (2.79 Å). This large value is indicative of a weak van der Waals bond, which explains why V_2O_5 presents an easy cleavage parallel to the (001) plane.[41] On the basis of their coordination number, three different types of lattice oxygen are present in this structure, namely, the singly coordinated vanadyl O(1), the doubly coordinated bridging O(2), and the triply coordinated bridging oxygen O(3).

On the other hand, anatase TiO_2 belongs to the *I*41/*amd* (D_{4h}^{19}) space group with experimental lattice constants $a = b = 3.787$ Å and $c = 9.515$ Å.[42] Its unit cell, Ti_4O_8, comprises four formula units. The structure can be described as composed of distorted TiO_6 octahedra with two different Ti−O distances, a long one (1.98 Å) involving the two apical oxygens and a short one (1.93 Å) involving the four equatorial oxygens. In this bulk structure (Figure 3), there is only one type of lattice oxygen (i.e., O(3)), which is coordinated to three titanium atoms.

In order to find the equilibrium volume and the bulk modulus of these systems at zero pressure and temperature, the unit cells of these bulk structures have been optimized at several volumes and the results have been fitted to a Murnaghan equation of state[43]

$$E(V) = E_0 + \frac{B_0 V}{B_0'}\left(\frac{(V_0/V)^{B_0'}}{B_0'-1} + 1\right) - \frac{B_0 V_0}{B_0'-1} \quad (6)$$

where V_0 and E_0 are the equilibrium volume and energy, respectively, B_0 is the bulk modulus at zero pressure, and B_0' is the bulk modulus pressure derivative. This fit for both of the materials is depicted in Figure S1 of the Supporting Information. Finally, an additional optimization is performed for each bulk

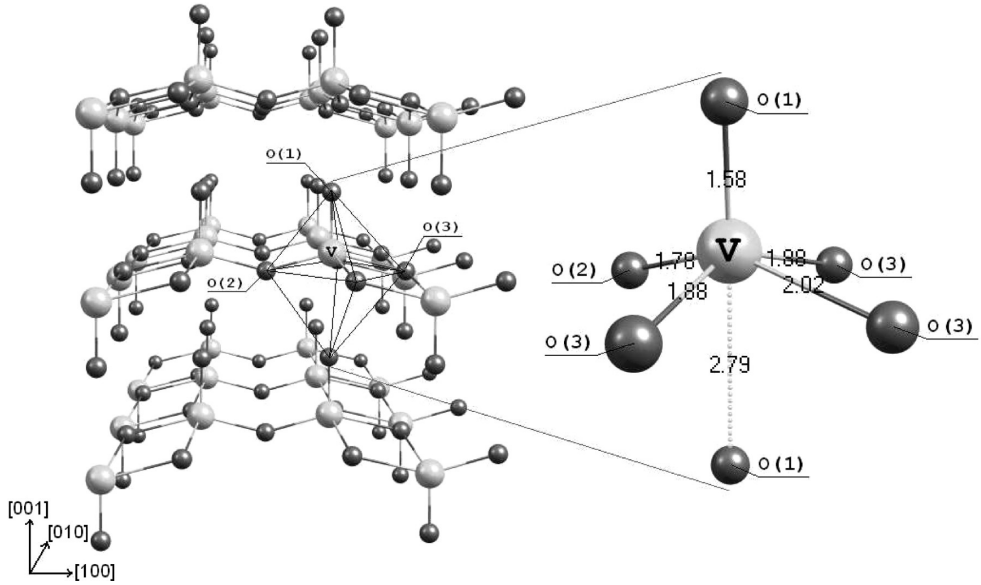

Figure 2. Crystal structure of V_2O_5 and its inequivalent oxygen atoms.

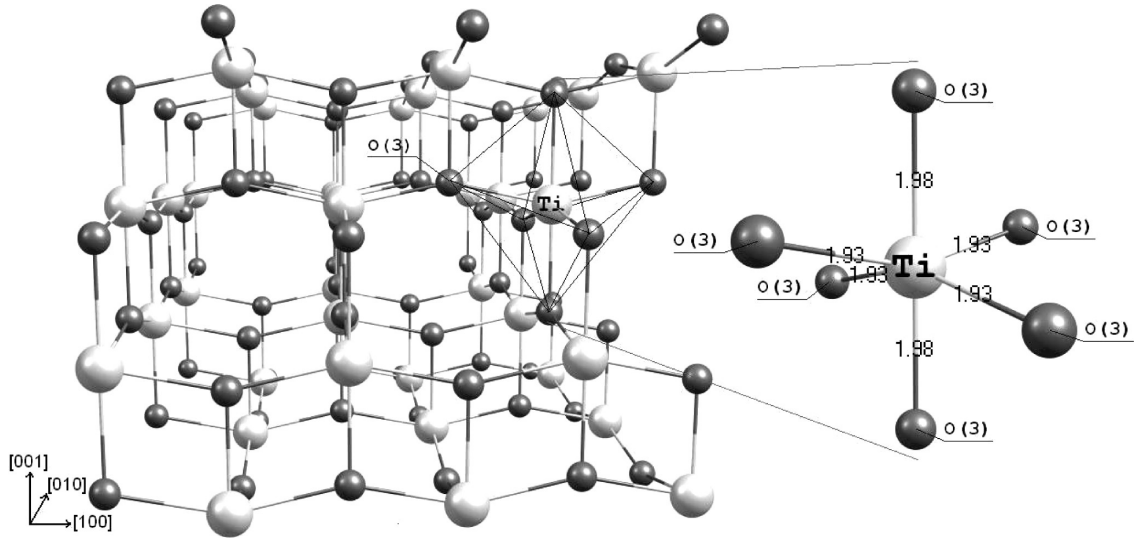

Figure 3. Crystal structure of TiO_2 anatase.

material at its equilibrium volume, in order to determine the optimum lattice constants and atomic positions.

(001) V_2O_5 Surface. Because V_2O_5 presents an easy cleavage parallel to the (001) plane, this plane has been used in this study to model the fully oxidized unsupported vanadia surface. However, when considering the (001) V_2O_5 surface, an additional distinction between the oxygen sites within the surface layer has to be made, owing to the differences in their surface orientation. As seen in Figure 4, six distinct oxygen sites exist within a (001) V_2O_5 layer: singly coordinated O(1)/O(1)′ belonging to a vanadyl group that is either sticking out of the surface or pointing into the bulk, respectively, doubly coordinated O(2)/O(2)′ bridging two vanadyl groups that are either pointing into the bulk or sticking out of the surface, respectively, triply coordinated O(3)/O(3)′ connecting either two vanadyl groups pointing into the bulk and one vanadyl group sticking out of the surface or vice versa. Due to this surface site orientation, the nonaccented oxygen sites are the ones that are easily accessible to gas-phase molecules and can be considered as active. On the other hand, the inaccessible sites O(1)′ are involved in the anchoring of the vanadia overlayer on the substrate, as will be seen in the modeling of the supported vanadia surface.

Periodic calculations have been performed for the (001) V_2O_5 surface using both single layer (V_2O_5 slab) and double layer ($V_2O_5-V_2O_5$ slab) slabs, in order to test whether there is any influence of a second underlying vanadia layer on the surface properties. In addition, for the cluster calculations, the $V_{10}O_{31}H_{12}$ (V10) cluster has been used as a realistic model of the (001) V_2O_5 surface, as suggested by Hermann et al.[44]

Weak Interaction Model: One-Layer (001) V_2O_5/(001) TiO_2 Anatase. The first type of supported models originates from the idea that a fully oxidized vanadia monolayer maintains more or less its crystallographic V_2O_5 structure when supported on titania anatase, which has been supported by experimental evidence.[13] As the interface between the (001) V_2O_5 monolayer and (001) TiO_2 surface exhibits a very small lattice misfit, it has been chosen for this kind of modeling. While the surface unit cell of (001) TiO_2 is tetragonal ($a = b = 3.79$ Å), the surface unit cell of (001) V_2O_5 is rectangular ($a = 11.51$ Å, $b = 3.56$ Å). For this reason, two possible orientations of (001) V_2O_5 on (001) TiO_2 have been considered, as shown in Figure

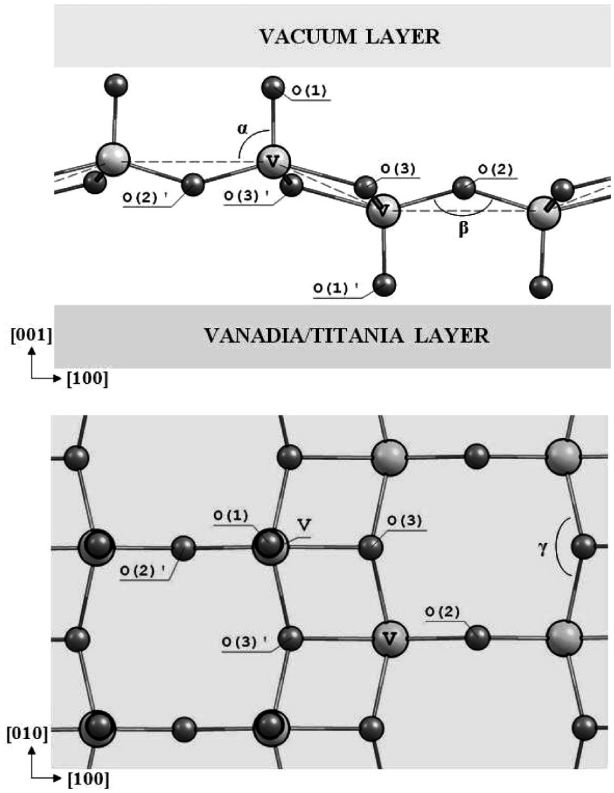

Figure 4. Side and top view of the (001) V_2O_5 surface. Oxygen sites with different coordination (number in parentheses) and different surface orientation (accented or not) are depicted. Certain angles used in Table 3 are also depicted. A dashed line has been drawn on the side view to differentiate between the oxygen sites that are pointing into the substrate and the ones that are pointing toward the vacuum and are easily accessible to gas-phase molecules.

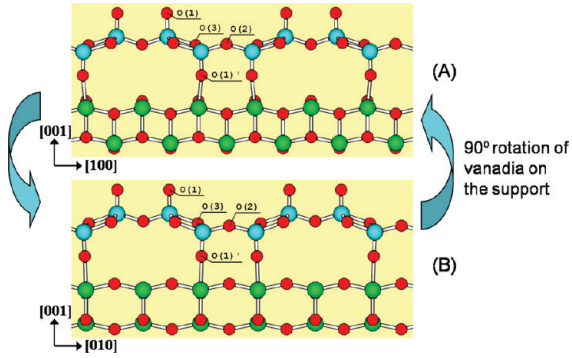

Figure 5. V_2O_5−TiO_2 slabs. Side view of the two possible orientations of a (001) V_2O_5 monolayer supported on (001) TiO_2 anatase (weak interaction with support). Blue balls are vanadium atoms, red balls are oxygen atoms, and green balls are titanium atoms.

5 (V_2O_5−TiO_2 slabs). As seen in this figure, the vanadia overlayer is anchored to the titania substrate using half of its vanadyl groups. Apart from the regions where bonding between vanadia and titania takes place, there are also large empty cavities below the vanadia overlayer at the regions where the vanadyl groups are sticking out of the surface, which is due to the alternating orientation of the double vanadyl rows on the vanadia overlayer structure. In addition to the periodic slabs for this kind of modeling, a series of cluster calculations have been performed using several cluster models of vanadia on titania (see Figure S2 of the Supporting Information). These clusters differ in size and in orientation of the active phase on the support, so that both effects can be studied for this type of modeling. However, due to the prerequisite of fixing the terminating H atoms, the optimum distance between the vanadia and titania cluster must be found manually before optimizing the positions of the atoms in the vanadia layer. This is simply done by choosing some points with different Ti−O(1)′ distance and calculating the energy of the system, with the optimum distance being the one minimizing its formation energy ($\Delta E_{f(cluster)}$). As seen in Figure S3 of the Supporting Information, a minimum in the formation energy of the supported cluster has been found, with the optimized Ti−O distance being 2.25 Å, which is equal to the distance obtained from the periodic calculations for the respective slab model (V_2O_5−TiO_2 (B) orientation). Additionally, in order to select the cluster that yields converged results for this surface system, the dependence of the properties on the cluster size has been examined. As seen from Table S1 of the Supporting Information, the data are almost identical for the two largest clusters (i.e., V10 on Ti10 (B) and V10 on Ti15 (A)), indicating that convergence of the electronic and energetic properties is achieved for the V10 on Ti10 cluster which is used in the following discussion.

Strong Interaction Model: One-Epitaxial Layer V_2O_5/(001) TiO_2 Anatase. The second approach for modeling the V_2O_5 monolayer supported on (001) TiO_2 anatase is based on results obtained by several surface characterization techniques[14] and assumes that the presence of the titania anatase support alters significantly the structure of the fully oxidized vanadia monolayer. This model is constructed by placing half monolayer of oxygen atoms on top of a pseudomorphic VO_2 phase that extends the (001) TiO_2 anatase structure. As illustrated in Figure 6, three possibilities of arranging these on-top oxygen atoms have been envisaged: one along the diagonal [110] direction (configuration A), one along the [100] direction (configuration B), and one along the [010] direction (configuration C). The resulting structures (VTiO slabs) are also shown in this figure after allowing the vanadia overlayer to relax. In addition to the periodic slabs for this kind of modeling, a series of cluster calculations have been performed using cluster models of different size (see Figure S4 of the Supporting Information). In order to select the cluster that can adequately describe this surface system, the convergence of the properties with cluster size has been examined. As seen from Table S2 of the Supporting Information, the data at all levels of analysis are identical for the two largest clusters (i.e., V4_Ti15 and V6_Ti16). Convergence of the electronic and energetic properties is thus achieved for the V4_Ti15 cluster, which is used in the following discussion.

Results and Discussion

Bulk V_2O_5 and TiO_2 Anatase. As seen in Tables 1 and 2, the calculated values of the lattice parameters, atomic positions, and bulk moduli are in good agreement with the experimental values.[40,42,45,46] This is an indication that both systems are well represented using the aforementioned computational methodology.

After the optimization of the bulk structure of V_2O_5 and TiO_2 anatase, band structure calculations have been performed in order to map the electronic structure of these systems. From the total spin-up and spin-down density of states (DOS) as plotted in Figures S5 and S6 for V_2O_5 and TiO_2, respectively, the diamagnetic character of both materials is observed. For V_2O_5 (Figure S5 in the Supporting Information), three characteristic groups of bands are identified around the Fermi level. A valence band that consists mainly of O 2p states with non-negligible V 3d contributions is found below the Fermi level. The calculated valence bandwidth of 4.9 eV is in good

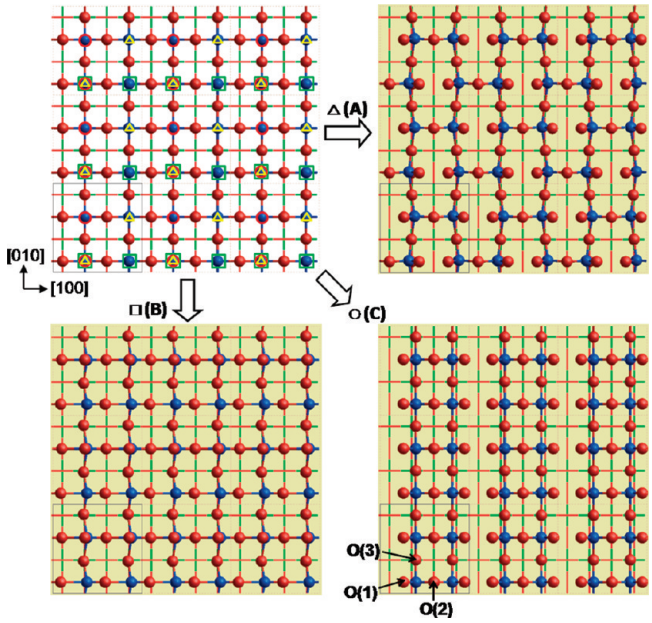

Figure 6. VTiO slabs. Schematic representation of different possibilities of arranging a half monolayer of oxygen atoms on top of a pseudomorphic VO_2 phase that extends the (001) TiO_2 anatase (white background) and top view of the resulting models (shaded background) representing an epitaxial monolayer of V_2O_5 supported on (001) TiO_2 anatase (strong interaction with support). The vanadia overlayer is represented by a ball and stick model, where the blue balls are the vanadium atoms and the red balls are the oxygen atoms, whereas the titania anatase support is depicted as a stick model with red indicating oxygen and green indicating titanium.

TABLE 1: Experimental versus Calculated Structural Parameters for Bulk V_2O_5

	experimental	calculated
	Lattice Parameters (in Å)	
a	11.512[a]	11.658
b	3.564[a]	3.575
c	4.368[a]	4.485
	Wyckoff Positions (*x*,*y*,*z*)	
V	(0.10118, 0.25, −0.1083)[a]	(0.10179, 0.25, −0.1076)
O(1)	(0.1043, 0.25, −0.469)[a]	(0.1047, 0.25, −0.467)
O(2)	(0.25, 0.25, 0.001)[a]	(0.25, 0.25, −0.002)
O(3)	(−0.0689, 0.25, 0.003)[a]	(−0.0683, 0.25, 0.005)
	Bulk Modulus (in GPa)	
B_0	50 ± 2[b]	49

[a] Reference 40. [b] Reference 45.

TABLE 2: Experimental versus Calculated Structural Parameters for Bulk TiO_2 Anatase

	experimental	calculated
	Lattice Parameters (in Å)	
a	3.787[a]	3.834
b	3.787[a]	3.834
c	9.515[a]	9.628
	Wyckoff Positions (*x*,*y*,*z*)	
Ti	(0, 0.75, 0.1250)[a]	(0, 0.75, 0.1250)
O(3)	(0, 0.75, 0.3333)[a]	(0, 0.75, 0.3328)
	Bulk Modulus (in GPa)	
B_0	179 ± 2[b]	174

[a] Reference 42. [b] Reference 46.

agreement with the experimental value of 5.5 eV reported in literature[49,50] (see Table 3). Above the Fermi level, the conduction band, which is mainly dominated by unoccupied V 3d states, is divided into two groups of bands: a narrow feature at lower energies separated from the broad upper group of bands by a gap of 0.6 eV. This split-off feature at the bottom of the conduction band consists of a pair of localized bands, and its existence has been reported in the literature by several authors.[40,49,51,52] Experimentally, V_2O_5 is considered to be a semiconductor with a band gap of about 2.3 eV.[48] In agreement with this, the periodic calculations for bulk V_2O_5 yield a direct band gap of 2.2 eV at the Γ-point and an indirect band gap of 1.7 eV that corresponds to a transition between the valence band maximum (located close to R along the RZ direction) and the conduction band minimum (located at the Γ-point). However, it has to be kept in mind that despite of this agreement, pure DFT methods in general underestimate the band gap of bulk materials.[49,53,54] This is evident in the case of TiO_2 anatase (Figure S6 in the Supporting Information), where the periodic calculations yield a direct band gap of 2.0 eV at the Γ-point and an indirect band gap of 1.9 eV corresponding to a S to Γ transition, while the experimental band gap is 3.2 eV.[54,55] Nevertheless, the calculated band gap is in agreement with other reported calculations.[53−56] In addition, the calculated valence bandwidth of 4.6 eV for bulk TiO_2 anatase agrees well with the experimental value of 4.75 eV, as obtained from XPS measurements.[55,56] Similar to V_2O_5, the valence band of TiO_2 anatase consists mainly of O 2p states with non-negligible Ti 3d contributions located at the bottom of the valence band, while the conduction band is dominated by unoccupied Ti 3d states.

By comparing the magnitude of the calculated charges on the V, O and Ti atoms for bulk V_2O_5 and TiO_2 anatase (see Table 4) with their formal charges (namely, +5, −2, and +4, respectively), it is found that these systems cannot be considered as purely ionic and exhibit also a covalent character. This is in line with a recent experimental study,[57] where the electronic structure of V_2O_5 has been probed by resonant photoemission spectroscopy (RPES). RPES results showed that the approximate charge on the V ion and the O ion in V_2O_5 is +3 and −1.2, respectively, indicating that the simple ionic model of bonding is not valid for such a system.

Overall, with the exception noted earlier, the present calculations describe well the geometric and electronic features of these well-defined bulk materials.

Unsupported V_2O_5 Surface. As seen in Tables 3 and 4 (bulk V_2O_5 vs V_2O_5 slab), when the bulk structure is cleaved to create the (001) V_2O_5 surface, no major surface relaxations and charge redistributions occur. A very small surface energy of 0.038 J/m^2 is calculated for the relaxed surface slab (Table 5), which is in good agreement with the reported values[41,58] of 0.040 and 0.047 J/m^2. In accordance with literature,[41,58] the V═O(1) bond lengths are shorter compared to the calculated bulk structure by less than 0.01 Å, while the V−O(2) and V−O(3) bond lengths are larger by the same amount (Table 3). In agreement with the periodic calculations of Yin et al.,[59] when going from bulk to one-layer V_2O_5 (Table 4), the negative charge of O(1) slightly decreases from −0.53 to −0.47 whereas the charges of O(2) and O(3) slightly increase from −0.80 to −0.83 and from −0.93 to −0.95, respectively, while the positive charge of V slightly decreases from +1.86 to +1.83. The band structure of the single (001) V_2O_5 slab (Figure S7 of the Supporting Information) resembles much the band structure of bulk V_2O_5 (Figure S5 of the Supporting Information), which is to be expected since the interaction between layers in V_2O_5 is so weak and all atoms within the (001) layer are coordinatively saturated. However, it is worth noting that the states of the single surface layer have somewhat less dispersion, i.e., they form narrower bands, as

TABLE 3: Calculated Bond Distances, Angles, and Band Structure for the Periodic Models Considered in This Study Compared to the Experimental Values of Bulk V_2O_5

		calculated				
	experimental (bulk V_2O_5)	V_2O_5 bulk	V_2O_5 slab	$V_2O_5-V_2O_5$ slab	$V_2O_5-TiO_2$ slab (A)	VTiO slab (C)[a]
			Bond Length (Å)			
V═O(1)	1.58	1.61	1.60	1.60	1.60	1.60 (1.58)
V−O(2)	1.78	1.79	1.80	1.80	1.82	1.77 (1.77)
V−O(3)[b]	1.88/2.02	1.89/2.05	1.90/2.06	1.89/2.08	1.99/1.99	1.96/1.97[c] (1.95/2.00[c])
			Bond Angle (deg)			
V···V═O(1)[d]	89	89	89	89	89	132
V−O(2)−V[e]	149	149	146	146	148	125
V−O(3)−V[f]	143	143	141	142	149	155
interlayer distance (Å)	O(1)···V, 2.79	O(1)···V, 2.87		O(1)′···V, 2.89	O(1)′−Ti, 2.22	O(3)−Ti, 1.97
			Band Structure (eV)			
Fermi level	-6.7 ± 0.1[g]	−8.8	−8.5	−8.4	−6.8	−7.8
band gap (indirect/direct)	2.3 ± 0.1[h]	1.7/2.2	2.0/2.2	1.7/1.9	0/0.2	0.9/1.4
valence bandwidth	5.5 ± 0.5[i]	4.9	4.5	4.8	6.2	5.4

[a] Values in parentheses from ref 15. [b] Along [010] direction/perpendicular to [010] direction. [c] This bond length is between O(3) and the underlying titanium atom of the support. [d] This angle is between the vanadyl group and its next neighboring vanadium atom positioned along the [100] direction (see angle α of Figure 4). [e] Angle β of Figure 4. [f] This angle is between O(3) and its two next neighboring vanadium atoms positioned along the [010] direction (see angle γ of Figure 4). [g] Reference 47. [h] Reference 48. [i] Reference 49.

TABLE 4: Calculated Atomic Charges Originating from a Bader Analysis on the Periodic Models Considered in This Study

	model	$V^{=O(1)}/V^{=O(1)'}$	O(1)/O(1)′	O(2)/O(2)′	O(3)/O(3)′	Ti
bulk V_2O_5		1.86	−0.53	−0.80	−0.93	
bulk TiO_2					−0.96	1.93
V_2O_5 slab		1.83	−0.47	−0.83	−0.95	
V_2O_5-V_2O_5 slab	top layer	1.86/1.85	−0.49/−0.53	−0.82/−0.81	−0.94/−0.93	
	bottom layer (fixed)	1.85/1.93	−0.48/−0.62	−0.83/−0.80	−0.94/−0.93	
V_2O_5-TiO_2 (A) slab	vanadia overlayer	1.86/1.84	−0.48/−0.59	−0.84/−0.85	−0.96/−0.97	
	top titania layer (fixed)			−0.89	−0.91	1.97
	bottom titania layer (fixed)			−0.97	−0.98	1.92
VTiO (C) slab	vanadia overlayer	1.86	−0.49	−0.77	−0.96	
	top titania layer (fixed)			−0.99	−0.96	1.94
	bottom titania layer (fixed)			−0.98	−0.97	1.94

TABLE 5: Calculated Surface Energy (J/m^2) for the Unsupported (001) V_2O_5 Slab and Monolayer Formation Energies (J/m^2) for the Supported Periodic Models Considered in This Study

model	orientation	ΔE_{surf} (J/m^2)	$\Delta E_{f(surf)}$ (J/m^2)
V_2O_5 slab		0.038	
$V_2O_5-TiO_2$ slab	(A)		0.056
	(B)		0.070
VTiO slab	(A)		−0.622
	(B)		−0.055
	(C)		−0.698

compared to the bulk. For this reason, a slight decrease of the valence bandwidth from 4.9 to 4.5 eV and a slight increase of the indirect band gap from 1.7 to 2.0 eV is observed when going from bulk to one-layer V_2O_5 (Table 3). As for bulk V_2O_5, a direct band gap of 2.2 eV is calculated at the Γ-point and a split-off band is again witnessed at the bottom of the conduction band of the (001) V_2O_5 surface, being separated from the main conduction band by a gap of 0.6 eV. Overall, these results are in agreement with the aforementioned weak interlayer interactions in V_2O_5.

From Tables 3 and 4 (V_2O_5 slab vs $V_2O_5-V_2O_5$ slab) it can be seen that a single layer slab is adequate for modeling the (001) V_2O_5 surface, since no significant differences on the structural and electronic properties of the surface are found for a two-layer slab. The V═O(1) and V−O(2) bond lengths are exactly the same, while the V−O(3) bond lengths differ only by about 0.01 Å. On comparison of the atomic charges for the one-layer slab with the charges on the atoms exposed to the gas phase (i.e., $V^{=O(1)'}$, O(1), O(2), O(3)) for the top layer of the two-layer slab, very small differences of 0.01−0.03 are found.

In addition to the periodic approach, the properties of the unsupported vanadia surface have been studied using the V10 cluster (Figure 7).[44] Although the Bader analysis for the cluster yields slightly more localized atomic charges (i.e., of larger absolute magnitude, namely, about 0.2 larger for V and 0.1 larger for O) as compared with the Bader analysis for the periodic slab, the trends and differences that exist between inequivalent ions are maintained (see Tables 4 and 6). According to the Bader analysis, the charges on O(1), O(2), and O(3) are −0.52, −0.88, and −1.07, respectively, for the V10 cluster and −0.47, −0.83, and −0.95 for the V_2O_5 slab. In both cases (cluster/slab), the negative charges on the oxygen atoms increase in the following order, O(1) < O(2) < O(3), and the difference of the charges between the inequivalent oxygen atoms (e.g., O(1)−O(2), O(2)−O(3)) is within the same order of magnitude. From the calculation of the electrostatic potential for the V10 cluster, the location of the most negative electron potential is found to be close to the vanadyl oxygens, which is in agreement with the result obtained for the one-layer (001) V_2O_5 slab (Figure 8a vs Figure 9a). Moreover, the energy of the HOMO level for the V10 cluster (−8.3 eV, Table 6) is in good agreement with the calculated Fermi level of the one-layer V_2O_5 slab model (−8.5 eV, Table 3), while the band gap of the cluster (3.9 eV, Table 6) is larger than the one determined with the periodic approach (2.2 eV, Table 3). In agreement with the periodic calculations on the (001) V_2O_5 surface (Figure 10), the calculated

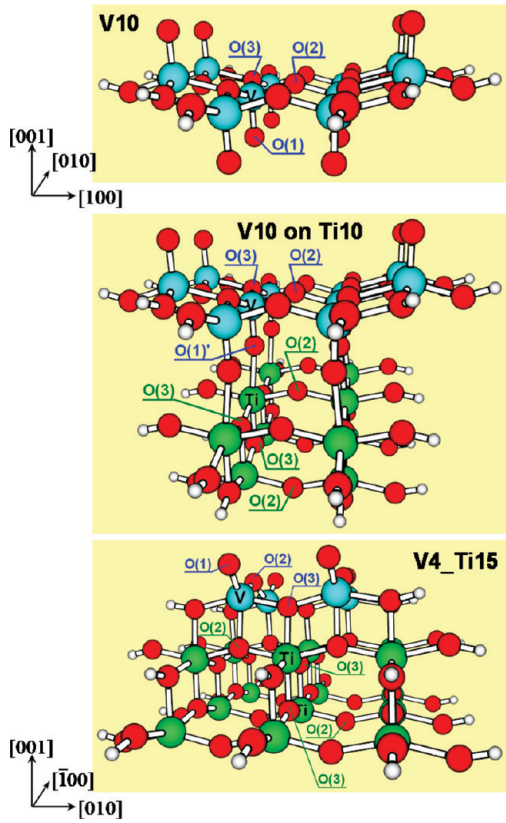

Figure 7. Size converged cluster models used to represent the (001) V_2O_5 surface (V10), a single layer of (001) V_2O_5 supported on (001) TiO_2 anatase (V10 on Ti10), and an epitaxial monolayer of V_2O_5 supported on (001) TiO_2 anatase (V4_Ti15).

DOS for the V10 cluster (Figure 11) shows that the valence band consists mainly of O states with non-negligible V contributions, while the conduction band is dominated by V providing unoccupied states to additional electrons, thus acting as Lewis acid sites. As seen in both cases from the projected DOS of Figures 10 and 11, the electronic states of O(1) are more localized in the center of the valence band having no contribution at the bottom of the valence band, while those of O(2) and O(3) are dispersed throughout the valence band with higher densities near its edges (i.e., close to the Fermi level and at the bottom of the valence band). Overall, there is a close resemblance of the properties of the V10 cluster compared to the V_2O_5 slab, thus justifying the modeling of the extended (001) V_2O_5 surface using such a cluster.

Therefore, the chemical bonding at this surface can be addressed using Wiberg bond order indices (Table 6) and projected DOS and COOP curves (Figure 11) calculated for the V10 cluster. According to the Wiberg bond order indices, the covalent nature of the bonds linking the different oxygen sites with their neighboring vanadium atoms decreases with coordination number. The total bond orders of 2.12 for O(1), of 1.84 for O(2), and of 1.62 for O(3) are in agreement with the corresponding increase of the ionic character of the oxygen center as expressed by the atomic charges, i.e., Bader charges of −0.52 for O(1), of −0.88 for O(2), and of −1.07 for O(3). In accordance with chemical intuition based on simple valence concepts, the Wiberg bond order analysis yields clearly a double bond (2.12) between V and O(1), two almost single bonds (0.92/0.92) linking O(2) to two V atoms, and three bonds, each being much weaker than a single bond (0.62/0.59/0.41), linking O(3) to three V atoms. In addition, using the COOP in conjunction with the DOS (Figure 11), the extent to which specific states contribute to a bond between atoms can be analyzed. It is worth noticing that in all cases the bonding contributions (positive COOP curve) arising from the hybridization of V and O states to form V−O bonds dominate the high energy region of the valence band and decrease when going toward the top of the valence band (close to the Fermi level), where the interaction appears to be slightly bonding for the V═O(1) pair, nonbonding (zero COOP curve) for the V−O(2) pair, and even slightly antibonding (negative COOP curve) for the V−O(3) pair. The

TABLE 6: Calculated Atomic Charges (q), Total Bond Orders (BO) per Atom and Energy Levels (HOMO, LUMO) for the Cluster Models Considered in This Study[a]

		vanadia overlayer				top titania layer			bottom titania layer					
model	electronic properties	V	O(1)/O(1)′	O(2)	O(3)	Ti	O(2)	O(3)	Ti	O(2)	O(3)	HOMO (eV)	LUMO (eV)	gap (eV)
V10	$q_{Mulliken}$	1.47	−0.29	−0.65	−0.89							−8.30	−4.40	3.90
	$q_{Roby-Davidson}$	1.71	−0.29	−0.72	−1.12									
	q_{Bader}	2.00	−0.52	−0.88	−1.07									
	$\sum(BO)_{Wiberg}$	4.68	2.12	1.84	1.62									
Ti10	$q_{Mulliken}$					1.72	−0.81	−0.88	1.70	−0.81	−0.89	−7.08	−3.27	3.81
	$q_{Roby-Davidson}$					1.15	−0.69	−0.37	1.16	−0.73	−0.41			
	q_{Bader}					2.08	−1.05	−1.01	2.11	−1.06	−1.00			
	$\sum(BO)_{Wiberg}$					3.47	1.65	1.78	3.47	1.65	1.78			
Ti15	$q_{Mulliken}$					1.69	−0.80	−0.92	1.72	−0.80	−0.91	−7.00	−3.21	3.78
	$q_{Roby-Davidson}$					1.09	−0.72	−0.58	1.09	−0.69	−0.56			
	q_{Bader}					2.09	−1.06	−1.01	2.07	−1.05	−1.01			
	$\sum(BO)_{Wiberg}$					3.42	1.66	1.77	3.42	1.66	1.77			
V10 on Ti10	$q_{Mulliken}$	1.59	−0.32	−0.66	−0.90	1.65	−0.71	−0.91	1.67	−0.82	−0.88	−6.17	−4.98	1.19
	$q_{Roby-Davidson}$	1.76	−0.33	−0.66	−1.07	0.86	−0.60	−0.54	1.06	−0.74	−0.61			
	q_{Bader}	2.12	−0.65	−0.87	−1.04	2.13	−1.01	−1.01	2.14	−1.08	−1.03			
	$\sum(BO)_{Wiberg}$	4.55	2.15	1.84	1.64	3.63	1.66	1.81	3.42	1.63	1.77			
V4_Ti15	$q_{Mulliken}$	1.38	−0.34	−0.56	−0.83	2.00	−0.96	−0.94	1.69	−0.80	−0.89	−7.11	−5.02	2.09
	$q_{Roby-Davidson}$	0.92	−0.20	−0.38	−0.66	0.88	−0.60	−0.46	1.12	−0.67	−0.50			
	q_{Bader}	2.03	−0.54	−0.86	−1.04	2.12	−1.05	−1.02	2.11	−1.07	−1.04			
	$\sum(BO)_{Wiberg}$	5.34	2.32	2.16	2.04	4.19	2.00	2.08	3.83	1.89	1.98			

[a] The values of the electronic properties are always taken from the atoms located at the center of the cluster (see Figure 7), as they are the most representative ones.

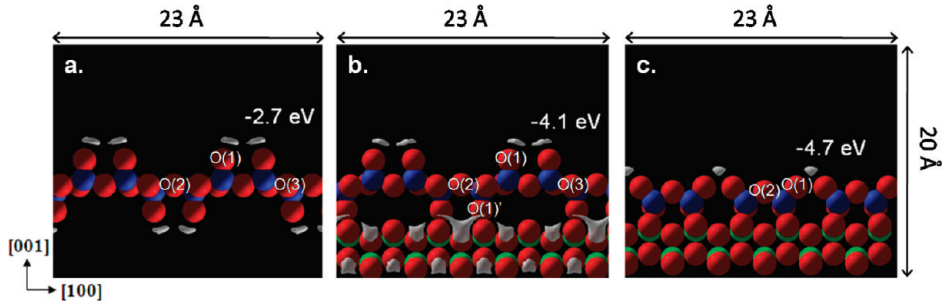

Figure 8. Isocontours (shown with white color) of the electrostatic potential calculated for the V_2O_5 (a), V_2O_5−TiO_2 (b), and VTiO (c) slab models. Blue balls are vanadium atoms, red balls are oxygen atoms, and green balls are titanium atoms.

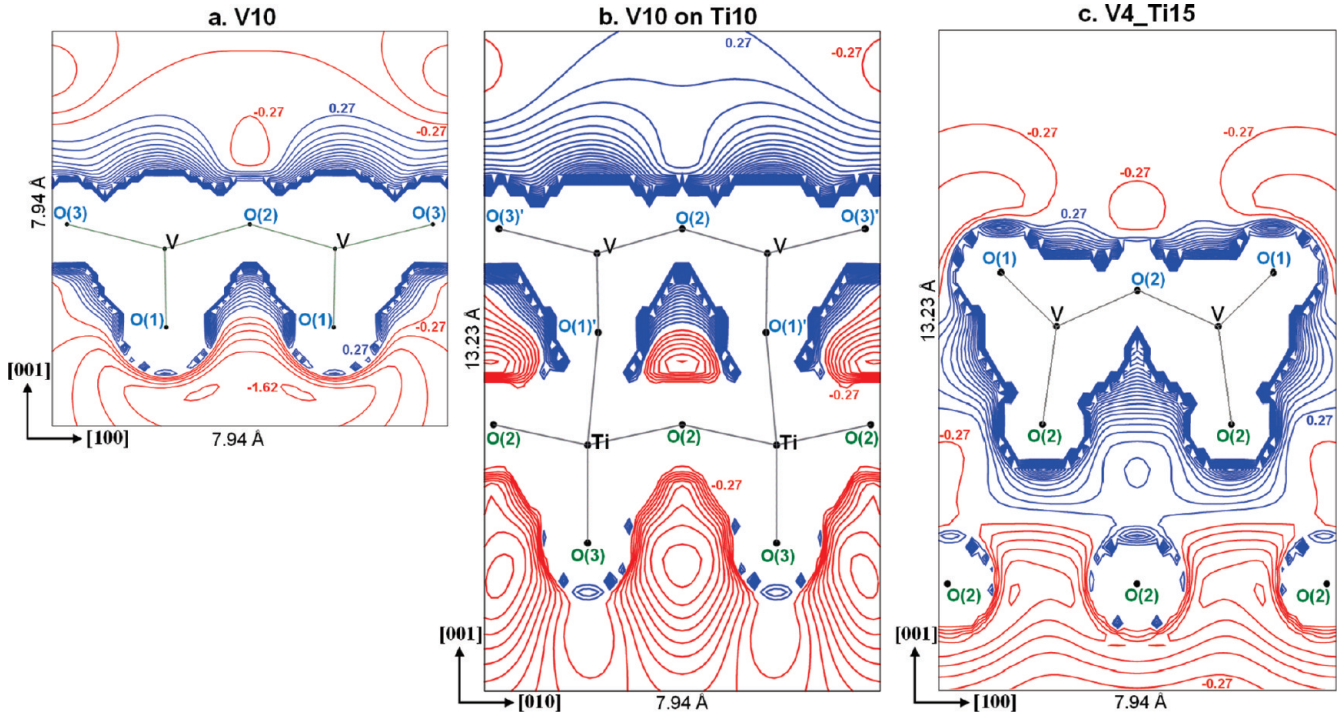

Figure 9. Contour plots of the electrostatic potential (values in electronvolts, contour increment 0.27 eV) for the unsupported V10 (a) cluster, and the supported V10 on Ti10 (b), and V4_Ti15 (c) clusters. Blue contours indicate a positive potential while red contours indicate a negative potential.

fact that there are almost no V states close to the Fermi level, while O states exist in this region, is indicative of the presence of oxygen lone pair electrons, which is responsible for the Lewis basic character of these oxygen centers. On the other hand, clear antibonding V−O states are observed above the band gap rising abruptly above the lower split-off band of the conduction band. The fact that no major antibonding V−O contributions are observed for this unoccupied split-off band shows that some additional electrons can be accommodated by the vanadia surface without influencing much its V−O bonds. These unoccupied V states are responsible for the Lewis acidity of the vanadia surface.

Supported V_2O_5 Surface: Weak Interaction with Support. As already mentioned in the methodology, two possible orientations of the vanadia monolayer on the titania support have been envisaged (see Figure 5). From the periodic calculations with these slab models, the following surface formation energies have been obtained at 0 K after relaxation of the vanadia monolayer (Table 5): $\Delta E_{f(surfA)} = 0.056$ J/m^2, $\Delta E_{f(surfB)} = 0.070$ J/m^2, and after including the relaxation of the top titania layer: $\Delta E_{f(surfA)} = 0.027$ J/m^2, $\Delta E_{f(surfB)} = 0.029$ J/m^2. This leads to the conclusion that there is almost no influence of the orientation of the active phase with respect to the support on the energetics of this system. Nevertheless, since orientation (A) is slightly more favorable based on the formation energies at 0 K, the V_2O_5−TiO_2 slab (A) has been chosen to analyze further the properties of this system when using the periodic approach. Moreover, as the relaxation of the top titania layer causes no significant changes in the geometry of the active phase and in the electronic properties of the supported system (see Table S3 of the Supporting Information), it has not been considered in the following discussion.

Some of the properties of the selected periodic model are summarized in Tables 3 and 4 together with the ones of the unsupported case (V_2O_5−TiO_2 slab (A) vs V_2O_5 slab). As seen in Table 3, compared to the unsupported vanadia slab, the V═O(1) bond length remains the same, the V−O(2) bond length increases slightly by 0.02 Å, while the largest structural change in the surface active sites is witnessed for O(3). Both bonds between O(3) and the vanadyl groups pointing into the substrate (V═O(1)′) are elongated by 0.09 Å, which is related to the fact that these vanadyl groups are weakly bonded with titania (Ti−O(1)′ interlayer bond of 2.22 Å), and this bond elongation is partially compensated by a bond contraction of 0.07 Å between O(3) and the vanadyl group sticking out of the surface. Overall, the structure of the supported vanadia overlayer in this

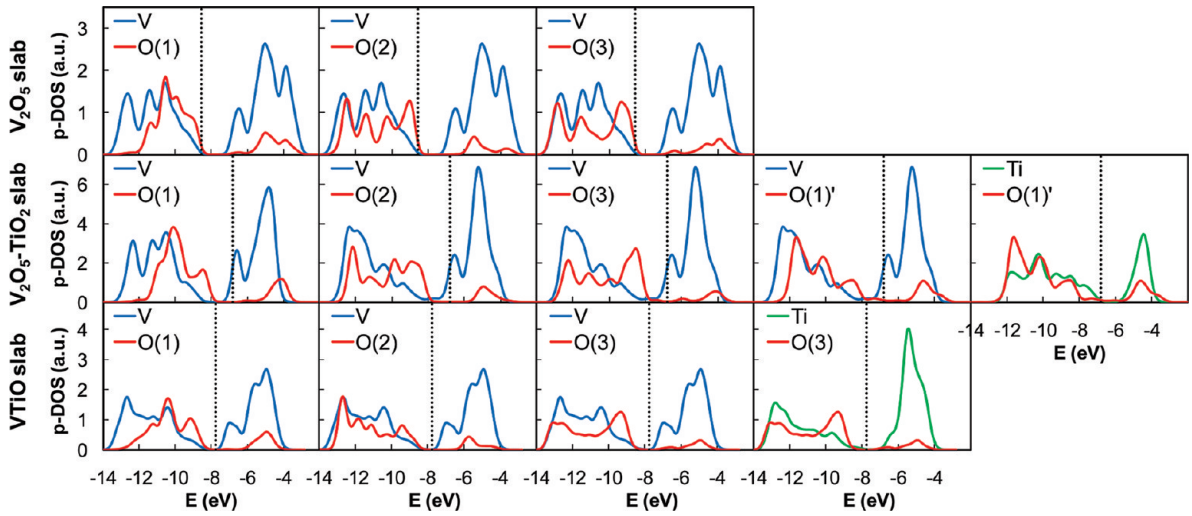

Figure 10. Projected DOS for the unsupported V_2O_5 slab and the supported $V_2O_5-TiO_2$ and VTiO slabs. In all cases, a Gaussian broadening of 0.5 eV is applied and the Fermi level is indicated by a dotted vertical line.

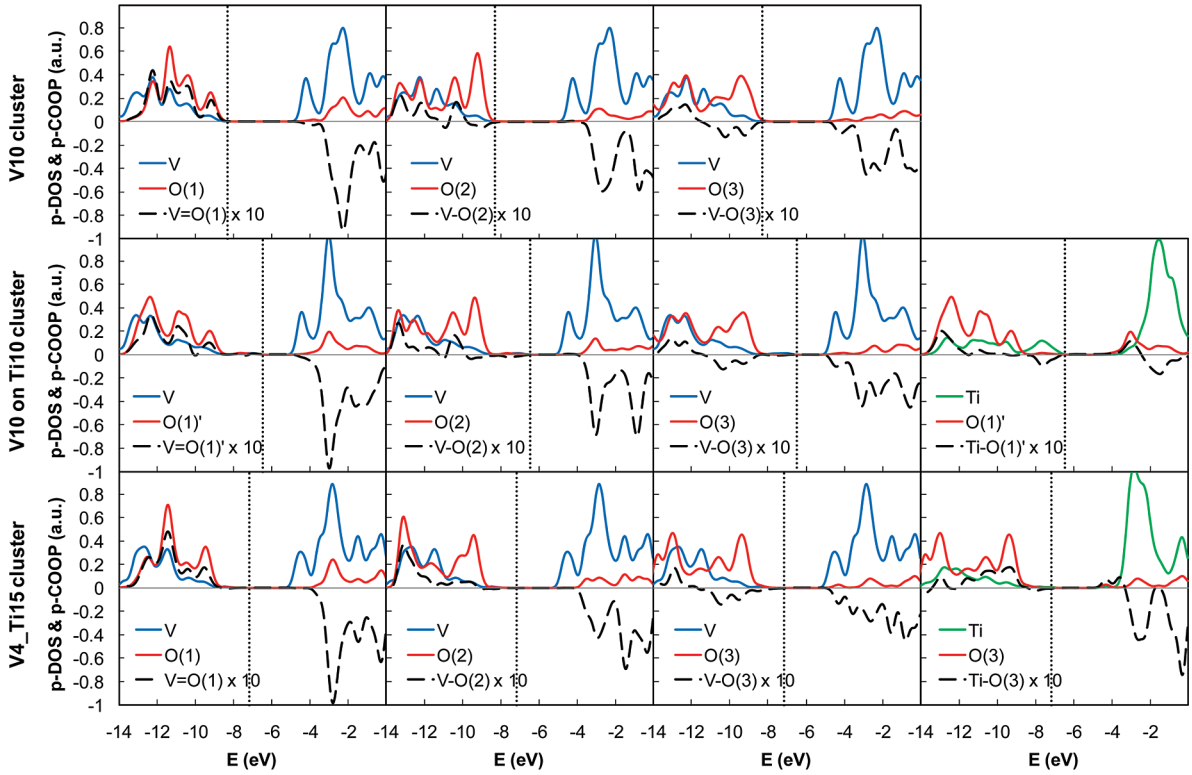

Figure 11. Projected DOS (full lines) and COOP (dashed lines) for the unsupported V10 cluster and the supported V10 on Ti10 and V4_Ti15 clusters. In all cases, a Gaussian broadening of 0.5 eV is applied and the Fermi level is indicated by a dotted vertical line.

model does not deviate much from the unsupported case, which is indicative of a weak interaction with the support. However, focusing on the electronic properties when going from the unsupported case to the supported case, certain changes can be observed, with the most obvious ones being related to the band structure. The direct band gap at the Γ-point for the supported slab (0.2 eV) is found to be 2.0 eV smaller than the one for the unsupported slab (2.2 eV), while no indirect band gap is observed for the supported slab as opposed to the unsupported case (2.0 eV). In addition, the Fermi level of the supported slab (−6.8 eV) moves to lower binding energies as compared to the one of the unsupported slab (−8.5 eV). This substantial decrease in the band gap together with the energy shift of the Fermi level can be an indication of a change in the reactivity of the surface. As seen from Figure S8 of the Supporting Information, due to the additional electronic states coming from the support, the number of bands has increased considerably, leading to an increase in the valence bandwidth (6.2 eV) as compared to the unsupported case (4.5 eV). Similar to the unsupported slab, the valence band of the supported slab mainly consists of O 2p states with non-negligible metal (V, Ti) contributions at the bottom of the band, whereas the conduction band is dominated by unoccupied metal (V, Ti) 3d states. While the unoccupied Ti 3d states are located well above the Fermi level at the top of the conduction band, the unoccupied V 3d states are located below the Ti 3d states at the bottom of the conduction band ending at the Fermi level. Compared to the unsupported vanadia slab, a split-off band is again witnessed at the bottom of the conduction band of the supported vanadia slab, only this time being located directly above the Fermi level and being separated

from the main conduction band by a gap of 0.5 eV, i.e., 0.1 eV smaller than for the unsupported case. As seen in Table 4, when going from the unsupported to the supported slab, the largest changes in the atomic charges are obtained for the oxygen atoms at the interface. A distinct example is the increase in the negative charge (from −0.47 to −0.59) of the vanadyl oxygen (O(1)′) of the vanadia overlayer which is bonded with the titania support. To obtain a more clear view of the charge redistribution induced by the weak interaction between vanadia and titania, the charge density difference (eq 4) is calculated for different regions of the $V_2O_5-TiO_2$ (A) slab model (see Figure 12, $V_2O_5-TiO_2$ slab). As seen from the magnitude of the plotted contours (part b vs c of Figure 12), most charge redistribution occurs in the bonding region between vanadia and titania. In this region (see Figure 12b), vanadia seems to be losing some charge density, especially from the V═O(1)′ bond, in order to create the new bond between O(1)′ and Ti. On the other hand, a small gain of electron density is observed close to the vanadyl oxygens (O(1)) that are pointing out of the surface (see Figure 12c). This is also evidenced by comparing the electrostatic potential maps of the unsupported and supported vanadia monolayer slabs. As seen in parts a and b of Figure 8, the magnitude of the negative electrostatic potential located above and in between the O(1) vanadyl oxygens increases upon deposition of vanadia on titania, i.e., −2.7 eV for the unsupported and −4.1 eV for the supported vanadia slab.

In addition to the periodic approach, the properties of the weak-interaction supported vanadia surface have been studied using the V10 on Ti10 cluster (Figure 7). The energy of the HOMO level for the V10 on Ti10 cluster (−6.2 eV, Table 6) is in good agreement with the calculated Fermi level of the $V_2O_5-TiO_2$ slab model (−6.8 eV, Table 3). The band gap of the cluster (1.2 eV, Table 6) is larger than the one determined with the periodic approach (0.2 eV, Table 3), which was also the case for the unsupported system and can be attributed to the hybrid nature of the functional used for the cluster calculations. A comparison between the slab calculation (Figure 10, $V_2O_5-TiO_2$ slab) and the cluster calculation (Figure 11, V10 on Ti10 cluster) yields very small differences in the valence band widths and qualitative agreement as to the energy variation of the p-DOS. Moreover, the charge density difference calculated for the slab model (Figure 12a, $V_2O_5-TiO_2$ slab) is very similar to the one calculated for the cluster model (Figure 12a, V10 on Ti10 cluster). The largest difference is seen for the orientation of the V 3d orbitals that are gaining electron density upon deposition of the vanadia monolayer on the titania support (i.e., d_{xy} for the slab vs d_{yz} for the cluster). According to the Bader analysis, the charges on O(1)′, O(2), O(3) of the vanadia overlayer are respectively −0.65, −0.87, −1.04 for the V10 on Ti10 cluster (Table 6), while the respective charges amount to −0.59, −0.84, −0.96 for the $V_2O_5-TiO_2$ slab (Table 4). Therefore, the trends and differences that exist between the inequivalent oxygen atoms are maintained in both modeling approaches (cluster and slab), and an overall close resemblance is found between the properties of V10 on Ti10 cluster vs $V_2O_5-TiO_2$ slab.

Comparing the supported cluster with the vanadia and titania clusters (V10 on Ti10 vs V10 and Ti10), it can be seen from the Mulliken population analysis in Table 6 that there is a charge transfer from vanadium, whose charge increases from +1.47 to +1.59, to titanium, whose charge decreases from +1.72 to +1.65, through the vanadyl oxygen sticking into the substrate, whose charge slightly increases from −0.29 to −0.32. Furthermore, to verify the results obtained from the atomic charges of the Mulliken population analysis, a modified Roby−Davidson population analysis based on occupation numbers was carried out. In contrast to the Mulliken population analysis, it is worth mentioning that based on the modified Roby−Davidson population analysis the calculated atomic charges on vanadium (+1.71) for the unsupported V10 cluster and on titanium (+1.15) for the Ti10 cluster agree with the order as expected from the formal oxidation states for these metal centers, i.e., V^{x+}, Ti^{y+} with $x > y$. However, when comparing the supported cluster with the vanadia and titania clusters, the modified Roby−Davidson population analysis points again to a charge transfer from vanadium, whose charge increases from +1.71 to +1.76, to titanium, whose charge decreases from +1.15 to +0.86, through the vanadyl oxygen sticking into the substrate, whose charge slightly increases from −0.29 to −0.33, all in agreement with the Mulliken population analysis. Moreover, when going from the unsupported to the supported system, the changes in the total bond orders per atom fully agree with the results previously obtained for the charge redistribution using either a Mulliken or a modified Roby−Davidson population analysis. The total bond order around vanadium decreases from 4.68 to 4.55, indicating a loss in electron density around this atom, while the total bond order per atom increases around titanium from 3.47 to 3.63 and around the vanadyl oxygen sticking into the substrate from 2.12 to 2.15, indicating a gain in electron density around these atoms. The new bond that is formed between O(1)′ and Ti is rather weak with a bond order of 0.23, while the V═O(1)′ bond is slightly weakened with a bond order of 1.92. The aforementioned charge depletion from vanadium followed by charge accumulation at the vanadia−titania interface is also indicated by the Bader analysis when going from the unsupported to the supported vanadia cluster. The positive charge on vanadium increases from +2.00 to +2.12 while the negative charge of the vanadyl oxygen sticking into the titania support increases from −0.52 to −0.65. However, a slight increase of the positive charge on titanium at the interface (from +2.08 to +2.13) is observed from the Bader analysis, which is in disagreement with what is found from the other three population analysis methods but is in good agreement with the loss of electron density around the titanium atom as witnessed from the charge density difference plot for this kind of system (see Figure 12b). Comparing the contour graphs of the electrostatic potential for the unsupported and supported vanadia cluster (parts a vs b of Figure 9), a small increase in the positive charge above the vanadium atoms is observed, which is in accordance with the loss of electron density in this region as witnessed from the charge density difference plot for this system (see Figure 12b). Finally, on comparison of the DOS and COOP curves between the V10 and the V10 on Ti10 cluster (Figure 11), it can be seen that most changes are observed for the occupied O(1)′ states whose stability increases after their interaction with the support, while the rest remain to a large extent the same. However, the most important change is the shift in the energy positions of the HOMO, from −8.3 to −6.2 eV, and of the LUMO, from −4.4 to −5.0 eV. As the LUMO eigenvalue corresponds to the energy change on addition of an incremental negative charge to the model and can be used as a measure of the Lewis acidity,[60] it can be concluded from the observed shift of the LUMO that the Lewis acidity of the vanadium atoms becomes stronger upon deposition of vanadia on titania, which is in agreement with the changes in the electrostatic potential (part a vs b of Figure 9) and with the charge redistribution calculated using atomic charges and charge density difference maps (Figure 12b).

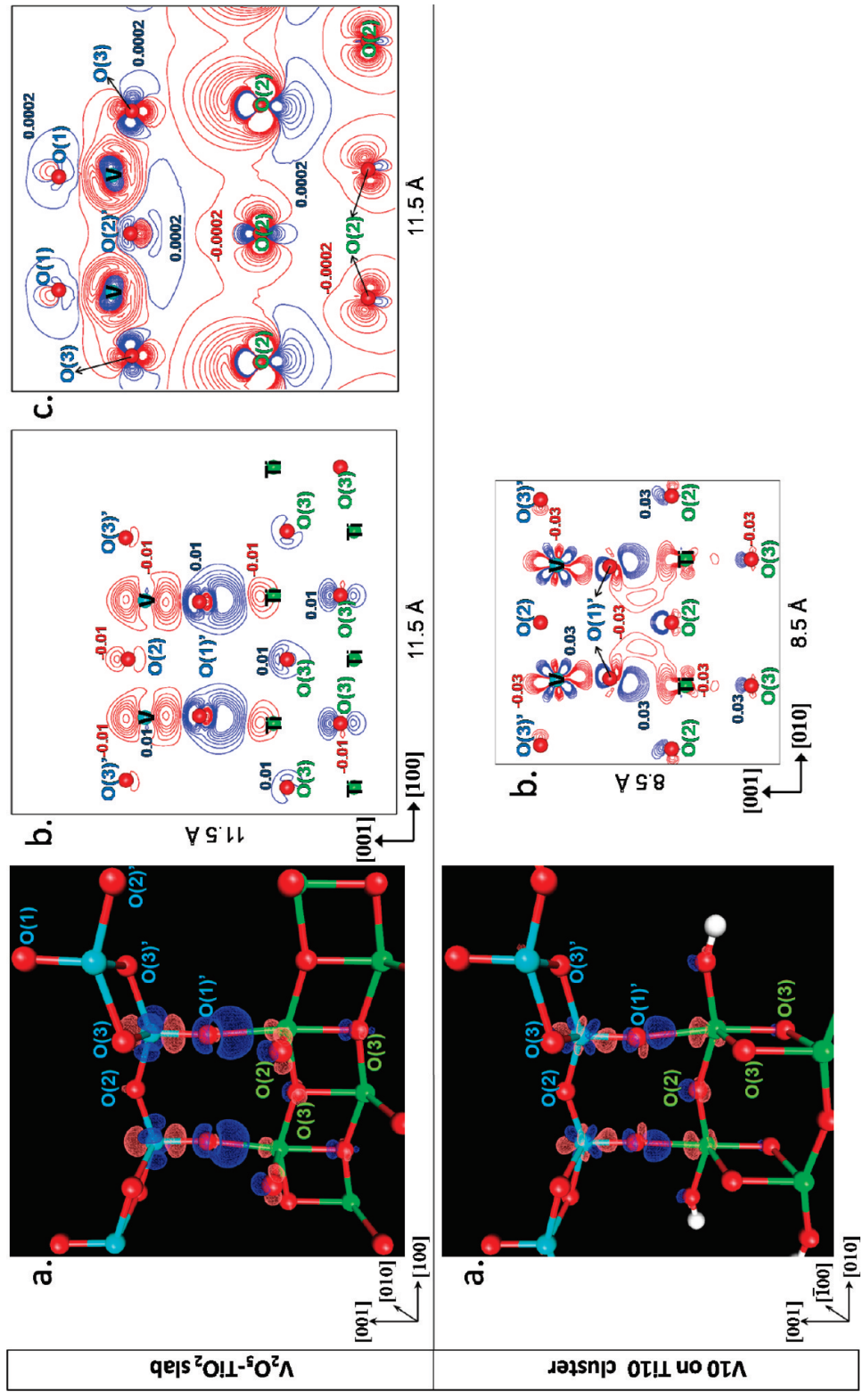

Figure 12. Charge density difference plot calculated according to eq 4 for the V_2O_5−TiO_2 slab model (a, isocontour value of 0.03 e/Å^3) and for the V10 on Ti10 cluster (a, isocontour value of 0.05 e/Å^3). Blue contours indicate a gain of electron density, while red contours indicate a loss of electron density. The contour maps are plotted for two regions (only the most representative one for the cluster model) where the vanadyl oxygens of the (001) V_2O_5 monolayer are pointing inward to the (001) TiO_2 anatase (b, contour increment 0.01 e/Å^3) and outward to the vacuum (c, contour increment 0.001 e/Å^3).

Supported V_2O_5 Surface: Strong Interaction with Support. As already mentioned, three possible configurations of the vanadia monolayer on the titania support have been investigated (see Figure 6). From the calculated surface formation energies at 0 K after relaxation of the vanadia monolayer of the slab models (Table 5), it is found that the most stable configuration is C with $\Delta E_{f(surfC)} = -0.698$ J/m^2, followed closely by configuration A with $\Delta E_{f(surfA)} = -0.622$ J/m^2, while configuration B with $\Delta E_{f(surfB)} = -0.055$ J/m^2 is the least stable. Including the relaxation of the top titania layer does not change this order in stability, yielding the following surface formation energies: $\Delta E_{f(surfA)} = -0.562$ J/m^2, $\Delta E_{f(surfB)} = -0.202$ J/m^2, $\Delta E_{f(surfC)} = -0.659$ J/m^2. Therefore, configuration C is chosen to represent the strong interaction model. Moreover, apart from a slight elongation of the V−O(3) distances, the relaxation of the top titania layer causes no other significant changes in the geometry of the active phase and in the electronic properties of the supported system (see Table S3 of the Supporting Information), and hence it has not been considered in the following discussion.

As seen from Figure 6, this fully oxidized vanadia monolayer is composed of O(1)═V−O(2)−V═O(1) groups which are connected to each other along the [010] direction via surface O(3) sites, thus forming rows along this direction. Apart from bridging two vanadium atoms, the triply coordinated surface O(3) sites are also bonded to the underlying titanium atoms of the support. The vanadium atoms are coordinated to four oxygen atoms within the vanadia overlayer (i.e., one O(1), one O(2), and two O(3)) and to one O(2) atom of the (001) TiO_2 support, keeping the coordination number to five. The strong interaction between the vanadia monolayer and the support leads to a much higher epitaxy as compared to the weak interaction model discussed above. It is worth mentioning that Vittadini and Selloni,[15] using theoretical calculations with a different approach for the construction of the model, i.e., via polymerization of vanadia monomers followed by elimination of the residual surface OH groups, reported a structure for the supported monolayer V_2O_5 that is in accordance with what is found in the present study. As illustrated in Table 3, similar bond lengths were obtained by Vittadini and Selloni.[15] Overall, by comparing the surface formation energies (Table 5), it can be concluded that this configuration, i.e., VTiO slab (C), is at 0 K the most favorable structure for the oxidized vanadia monolayer among the investigated interface models.

The properties of the selected periodic model are summarized in Tables 3 and 4, where distinct differences with the other models can be observed (VTiO slab (C) vs V_2O_5−TiO_2 slab (A) and/or V_2O_5 slab). As seen in Table 3, although the V═O(1) bond lengths for this model are the same as for the unsupported and supported (001) V_2O_5 surface (1.60 Å in all cases), the vanadyl groups in this case are tilted, i.e., V···V═O(1): 132° in the VTiO slab instead of 89° in both V_2O_5 and V_2O_5−TiO_2 slab. Moreover, the V−O(2) bonds of the VTiO slab are shorter (1.77 Å in the VTiO slab, 1.80 Å in the V_2O_5 slab, and 1.82 Å in the V_2O_5−TiO_2 slab) and thus stronger compared to the other two cases. In addition, the V−O(3) bond lengths along the [010] direction scale as follows for the different surface models: 1.90 Å (V_2O_5) < 1.96 Å (VTiO) < 1.99 Å (V_2O_5−TiO_2), with their strength increasing in the opposite manner. As a sign of stronger interaction between the vanadia monolayer and the titania support, the interlayer distance of the VTiO slab is shorter (1.97 Å) than the one of the V_2O_5−TiO_2 slab (2.22 Å). The most characteristic features obtained from the band structure calculations are also reported in Table 3, where a shift in the Fermi level to lower binding energies (from −8.5 to −7.8 eV) is observed when comparing the unsupported V_2O_5 with the supported VTiO model. The direct band gap at the Γ-point for the VTiO slab (1.4 eV) is found to be 0.8 eV smaller than the one for the unsupported slab (2.2 eV), while the indirect band gap for the supported slab (0.9 eV, corresponding to a Y → Γ transition) is found to be 1.1 eV smaller than the one for the unsupported case (2.0 eV, corresponding to a R → Γ transition). As seen from Figure S9 of the Supporting Information, similar to the V_2O_5 and V_2O_5−TiO_2 slab, the valence band of the supported VTiO slab is mainly occupied by O 2p states with non-negligible metal (V, Ti) contributions at the bottom of the band, while the conduction band is dominated by unoccupied metal (V, Ti) 3d states. Like the V_2O_5−TiO_2 slab, the bottom of the conduction band is dominated by empty V 3d states. Therefore, both weak and strong interaction between the two phases result in a smaller band gap for the supported system, while empty vanadium levels are located below the ones belonging to titanium, in agreement with what has been reported by Haber and Witko[61] for the V_2O_5/TiO_2 system. A noticeable difference between the two cases of the supported vanadia monolayer is that the weak interaction model exhibits a wider valence band (6.2 eV) than the strong interaction model (5.4 eV), which can be attributed to less mixing of bands between the vanadia and the titania phase resulting in a more or less simple superposition of bands that is indicative of the weak interaction between these two phases. Compared to the V_2O_5 and the V_2O_5−TiO_2 slab, a split-off band is again witnessed at the bottom of the conduction band of the VTiO slab, only this time being separated from the main conduction band by a much smaller gap (0.05 eV) than in the case of the unsupported (0.6 eV) and supported (001) V_2O_5 surface (0.5 eV). The results of the Bader analysis are summarized in Table 4, where no significant differences in the charges of the surface oxygen atoms exist between the V_2O_5, V_2O_5−TiO_2, and VTiO slab, with the largest change being a decrease in the charge of the O(2) site when going from V_2O_5 (−0.83) to VTiO (−0.77). However, as seen in Figure 8, the magnitude of the negative electrostatic potential located above and in between the vanadyl oxygens sticking out of the surface is not only increasing upon deposition of vanadia on titania (−2.7 eV for the unsupported V_2O_5 slab and −4.7 eV for the supported VTiO slab), but also increasing as the epitaxy of the monolayer on the support becomes higher (−4.1 eV for the supported V_2O_5−TiO_2 slab and −4.7 eV for the supported VTiO slab).

In addition to the periodic approach, the properties of the supported vanadia−strong interaction surface have been studied using the V4_Ti15 cluster (Figure 7). According to the Bader analysis, the charges on O(1), O(2), and O(3) of the vanadia overlayer are −0.54, −0.86, and −1.04, respectively, for the V4_Ti15 cluster (Table 6), while the respective charges are −0.49, −0.77, and −0.96 for the VTiO slab (Table 4). Therefore, the trends and differences that exist between the inequivalent oxygen atoms are maintained in both modeling approaches (cluster and slab). Moreover, from the calculation of the electrostatic potential for the V4_Ti15 cluster, the location of the most negative electron potential at the vanadia surface is found to be close to the vanadyl oxygens, which is in agreement with the result obtained for the VTiO slab (Figure 8c vs Figure 9c). The energy of the HOMO level for the V4_Ti15 cluster (−7.1 eV, Table 6) is in good agreement with the calculated Fermi level of the VTiO slab model (−7.8 eV, Table 3). The band gap of the cluster (2.1 eV, Table 6) is larger than the one determined with the periodic approach (1.4 eV, Table 3), which

TABLE 7: Calculated Hydrogen Adsorption Energies on Different Oxygen Sites and Models

	this work			Hermann et al.[a]	Yin et al.[b]	Goclon et al.[c]
ΔE_{ads} (kJ/mol)	V_2O_5 slab	$V_2O_5-TiO_2$ slab	VTiO slab	V10 cluster	V_2O_5 slab	$V_2O_5-V_2O_5$ slab
O(1) + H → O(1)*H	−277	−286	−340	−294	−271	−290
O(2) + H → O(2)*H	−268	−276	−260	−266	−253	−269
O(3) + H → O(3)*H	−252	−286	−265	−241	−249	−251

[a] Reference 44. [b] Reference 59. [c] Reference 62.

was also the case for the unsupported vanadia and for the supported vanadia−weak interaction model. Finally, a comparison of the slab calculation (Figure 10, VTiO slab) with the cluster calculation (Figure 11, V4_Ti15 cluster) yields very small differences in the valence band widths and qualitative agreement as to the energy variation of the p-DOS. Therefore, an overall close resemblance is found between the properties of V4_Ti15 cluster and the VTiO slab.

Further analysis using cluster calculations has been performed to compare the electronic and bonding properties of the V4_Ti15, V10 and V10 on Ti10 models. When going from V10 to V4_Ti15, a clear decrease of the magnitude of the atomic charges on vanadia occurs as calculated from the modified Roby−Davidson analysis (from +1.71/−0.29/−0.72/−1.12 at V10 to +0.92/−0.20/−0.38/−0.66 at V4_Ti15 for V/O(1)/O(2)/O(3), respectively). This is accompanied by a respective increase in the total Wiberg bond orders (from 4.68/2.12/1.84/1.62 at V10 to 5.34/2.32/2.16/2.04 at V4_Ti15 for V/O(1)/O(2)/O(3), respectively), thus enhancing the covalent character of the V−O bonding at the vanadia surface at the expense of the ionic bonding. By comparing the bond orders of the interlayer bonds for V4_Ti15 (0.68) and V10 on Ti10 (0.23), it is clear that the O(3)−Ti bond of V4_Ti15 is much stronger than the O(1)′−Ti bond of V10 on Ti10, justifying their characterization as models of strong and weak interaction with the support, respectively. Comparing the DOS and COOP curves between the V10 and the V4_Ti15 cluster, most changes in the shape of these curves are observed for the occupied O(2) states whose stability increases in accordance with the increase of the bond order of V−O(2) from 0.92 in V10 to 1.08 in V4_Ti15, while the rest remain to a large extent the same. However, the most important change is the shift in the energy positions of the HOMO from −8.3 to −7.1 eV and of the LUMO from −4.4 to −5.0 eV. Like in the case of the V10 on Ti10 cluster, the observed shift of the LUMO when going from the V10 to the V4_Ti15 cluster indicates that the Lewis acidity of the vanadia centers becomes stronger upon deposition of vanadia on titania, regardless of the way those two phases interact, i.e., weak or strong interaction. The increased acidity of the VO_x/TiO_2 catalyst system compared to pure V_2O_5 was also observed by Kachurovskaya et al.[6] using cluster models constructed by replacing a surface titanium atom by a vanadium atom.

Hydrogen Adsorption. As already mentioned there are several inequivalent active sites available on the vanadia surface. To test their reactivity for activating a C−H bond of a hydrocarbon, hydrogen adsorption has been used as a probe reaction.[22] However, it is worth mentioning that because the active phase is modeled as a vanadia monolayer, there are no V−O−Ti active sites, as proposed in literature for V_2O_5/TiO_2 catalysts with less than a monolayer of vanadia.[62] As shown in Table 7, for all sites of the supported and unsupported vanadia monolayer, hydrogen adsorption is an exothermic process. For the unsupported vanadia the adsorption energies at the different sites are in good agreement with other periodic and cluster calculations (see Table 7).[44,59,63] The vanadyl oxygen (O(1)) is

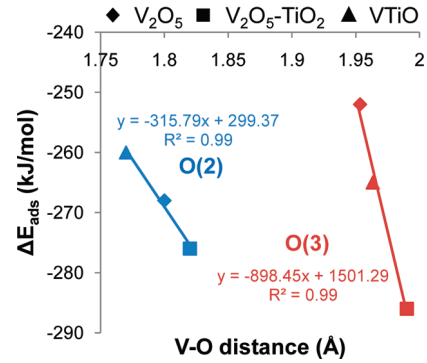

Figure 13. Calculated adsorption energy of hydrogen vs average V−O bond distance.

the most favorable one for H adsorption, and the adsorption energy on this site increases upon deposition of the vanadia monolayer on the titania anatase support and is further increased as a higher epitaxy of vanadia on titania is achieved (V_2O_5, −277 kJ/mol; $V_2O_5-TiO_2$, −286 kJ/mol; VTiO, −340 kJ/mol), which correlates well with the increase in the negative electrostatic potential above this site (see Figure 8). Interestingly enough, as mentioned in literature,[64] H adsorption on vanadia follows the same trend as H^+ adsorption, thus such a correlation is to be expected. On the bridging oxygen sites, O(2) or O(3), the observed trend in the adsorption energies when going from the unsupported to the supported vanadia correlates well with the V−O distances (Figure 13), since upon H adsorption these bonds have to be elongated. With this rationale, the shorter the bonds (i.e., V−O(2), 1.82 Å ($V_2O_5-TiO_2$) > 1.80 Å (V_2O_5) > 1.77 Å (VTiO); average V−O(3), 1.99 Å ($V_2O_5-TiO_2$) > 1.96 Å (VTiO) > 1.95 Å (V_2O_5)), the stronger they are and the more the energy that needs to be used to elongate them, thus yielding a lower adsorption energy (i.e., O(2), −276 kJ/mol ($V_2O_5-TiO_2$), −268 kJ/mol (V_2O_5), −260 kJ/mol (VTiO); O(3), −286 kJ/mol ($V_2O_5-TiO_2$), −265 kJ/mol (VTiO), −252 kJ/mol (V_2O_5)). Another possible and more general way of explaining the observed reactivity of the oxygen sites in H adsorption for the different catalyst models is in terms of frontier orbital analysis and models based on band-orbital mixing.[34,39] As the most important bonding interactions are between frontier orbitals, it can be expected that the adsorption energy of the same adsorbate (i.e., H) on the oxygen sites of the different catalyst models is related to the energy positions of the metal oxide's occupied and unoccupied states. Such a correlation is illustrated in Figure 14, where the calculated adsorption energy of H is plotted versus the band gap between the lowest unoccupied band, i.e., V_{t2g}, and the highest occupied band, i.e., O_p, for each oxygen site and different catalyst models. From this figure it is observed that the adsorption energy becomes more exothermic when the highest occupied oxygen band moves to lower binding energies and/or the lowest unoccupied vanadium band moves to higher binding energies. Finally, as seen in Table S3 of the Supporting Information, the additional relaxation of the topmost titania layer does not result in major

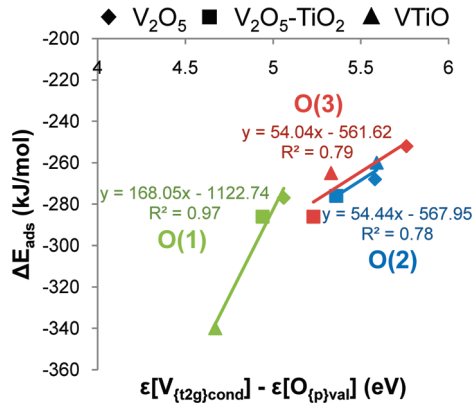

Figure 14. Calculated adsorption energy of hydrogen vs V−O band gap (between lowest unoccupied band, i.e., V_{t2g}, and highest occupied band, i.e., O_p, for each oxygen site), where ε corresponds to the energy position of the center of each band (estimated using the function centroid of the respective p-DOS curve).

changes in the adsorption energies of hydrogen, apart from an increase in the adsorption energy of 9 kJ/mol for the O(3) site of the VTiO (C) model.

Conclusions

Cluster and periodic DFT calculations have been performed to analyze the effect of (001) TiO_2 anatase support on the structure and properties of a fully oxidized V_2O_5 monolayer. Both theoretical approaches arrive at the same qualitative results. In accordance with experimental evidence, two different models of the monolayer V_2O_5/TiO_2 (anatase) catalyst have been investigated. In the first one, the vanadia monolayer maintains its crystallographic (001) V_2O_5 structure when supported on titania anatase. Although the interaction between the two phases is rather weak in this model, it is still enough to induce a charge redistribution that enhances the Lewis acidity of vanadium. In the second model, the presence of the titania anatase support alters significantly the structure of the fully oxidized vanadia monolayer, resulting in a stronger interaction and achieving a much higher epitaxy. On the basis of the surface formation energies at 0 K, the strong interaction model has the most favorable configuration for the structure of the supported oxidized vanadia monolayer.

The electronic structure of the investigated systems has been characterized in detail using band structure calculations. Compared to the unsupported vanadia, both weak and strong interaction models result in a shift of the Fermi level to lower binding energies together with a reduced band gap, which can lead to possible changes in the reactivity of the catalyst depending also on the adsorbate. In both cases, the shift of the lowest unoccupied V states to higher binding energies upon deposition of vanadia on titania indicates that the Lewis acidity of vanadium becomes stronger. Moreover, the electrostatic potential proves to be a useful reactivity descriptor, indicating the electron-rich regions. A hard electrophilic attack will occur close to the vanadyl oxygens for any case, while the deposition of a vanadia monolayer on titania anatase increases the chemical hardness of the vanadyl site for both weak and strong interaction models. It is also observed that the higher the epitaxy with the support, the more electron rich the vanadyl region is. Therefore, atomic hydrogen adsorption at 0 K is most favorable at the vanadyl site of the supported vanadia monolayer with the highest epitaxy. In conclusion, the observed reactivity of the oxygen sites in H adsorption for the different catalyst models correlates well with the energy positions of the frontier orbitals of the metal oxide, since the adsorption energy of H becomes more exothermic when the highest occupied oxygen band moves to lower binding energies and/or the lowest unoccupied vanadium band moves to higher binding energies.

Acknowledgment. The European Community (FP6 Network of Excellence IDECAT (NMP3-CT-2005-0113)) is acknowledged for financial support.

Supporting Information Available: Optimization of the unit cell volume of bulk V_2O_5 and TiO_2 anatase, optimization of the vanadia−titania distance using cluster calculations, band structures of the periodic models, overview of all cluster models used together with their electronic properties, effect of relaxation on geometric/electronic/energetic data obtained using periodic calculations, and atomic coordinates of the selected catalyst models. This material is available free of charge via the Internet at http://pubs.acs.org.

References and Notes

(1) Grzybowska-Swierkosz, B. *Appl. Catal., A* **1997**, *157*, 263.
(2) Bond, G. C. *Appl. Catal., A* **1997**, *157*, 91.
(3) Calatayud, M.; Minot, C. *Top. Catal.* **2006**, *41*, 17.
(4) Grzybowska-Swierkosz, B. *Top. Catal.* **2000**, *11*, 23.
(5) Avdeev, V. I.; Zhidomirov, G. M. *J. Struct. Chem.* **2005**, *46*, 577.
(6) Kachurovskaya, N. A.; Mikheeva, E. P.; Zhidomirov, G. M. *J. Mol. Catal. A: Chem.* **2002**, *178*, 191.
(7) Grybos, R.; Witko, M. *J. Phys. Chem. C* **2007**, *111*, 4216.
(8) Devriendt, K.; Poelman, H.; Fiermans, L. *Surf. Interface Anal.* **2000**, *29*, 139.
(9) Wachs, I. E. *Chem. Eng. Sci.* **1990**, *45*, 2561.
(10) Kozlowski, R.; Pettifer, R. F.; Thomas, J. M. *J. Phys. Chem.* **1983**, *87*, 5176.
(11) Carlson, T.; Griffin, G. L. *J. Phys. Chem.* **1986**, *90*, 5896.
(12) Sayle, D. C.; Catlow, C. R. A.; Perrin, M. A.; Nortier, P. *J. Phys. Chem.* **1996**, *100*, 8940.
(13) Silversmit, G.; van Bokhoven, J. A.; Poelman, H.; van der Eerden, A. M. J.; Marin, G. B.; Reyniers, M. F.; De Gryse, R. *Appl. Catal., A* **2005**, *285*, 151.
(14) Gao, W.; Wang, C. M.; Wang, H. Q.; Henrich, V. E.; Altman, E. I. *Surf. Sci.* **2004**, *559*, 201.
(15) Vittadini, A.; Selloni, A. *J. Phys. Chem. B* **2004**, *108*, 7337.
(16) Todorova, T. K.; Ganduglia-Pirovano, M. V.; Sauer, J. *J. Phys. Chem. B* **2005**, *109*, 23523.
(17) Kresse, G.; Hafner, J. *Phys. Rev. B* **1993**, *48*, 13115.
(18) Kresse, G.; Furthmuller, J. *Comput. Mater. Sci.* **1996**, *6*, 15.
(19) Blochl, P. E. *Phys. Rev. B* **1994**, *50*, 17953.
(20) Kresse, G.; Joubert, D. *Phys. Rev. B* **1999**, *59*, 1758.
(21) Perdew, J. P.; Burke, K.; Ernzerhof, M. *Phys. Rev. Lett.* **1996**, *77*, 3865.
(22) Witko, M. *Catal. Today* **1996**, *32*, 89.
(23) Monkhorst, H. J.; Pack, J. D. *Phys. Rev. B* **1976**, *13*, 5188.
(24) De Vita, A.; Gillan, M. J. *J. Phys.: Condens. Matter* **1991**, *3*, 6225.
(25) Vittadini, A.; Casarin, M.; Selloni, A. *Theor. Chem. Acc.* **2007**, *117*, 663.
(26) Bader, R. F. W. *Atoms in molecules: a quantum theory*; Clarendon Press: Oxford, 1990.
(27) Henkelman, G.; Arnaldsson, A.; Jonsson, H. *Comput. Mater. Sci.* **2006**, *36*, 354.
(28) Calatayud, M.; Tielens, F.; De Proft, F. *Chem. Phys. Lett.* **2008**, *456*, 59.
(29) Sauer, J.; Dobler, J. *Dalton. Trans.* **2004**, 3116.
(30) Ahlrichs, R.; Bar, M.; Haser, M.; Horn, H.; Kolmel, C. *Chem. Phys. Lett.* **1989**, *162*, 165.
(31) Treutler, O.; Ahlrichs, R. *J. Chem. Phys.* **1995**, *102*, 346.
(32) Deglmann, P.; Furche, F.; Ahlrichs, R. *Chem. Phys. Lett.* **2002**, *362*, 511.
(33) Schafer, A.; Huber, C.; Ahlrichs, R. *J. Chem. Phys.* **1994**, *100*, 5829.
(34) Rodriguez, J. A. *Theor. Chem. Acc.* **2002**, *107*, 117.
(35) Frisch, M. J.; Trucks, G. W.; Schlegel, H. B.; Scuseria, G. E.; Robb, M. A.; Cheeseman, J. R.; Montgomery, J. A., Jr.; Vreven, T.; Kudin, K. N. ; Burant, J. C.; Millam, J. M.; Iyengar, S. S.; Tomasi, J.; Barone, V.; Mennucci, B.; Cossi, M.; Scalmani, G.; Rega, N.; Petersson, G. A.; Nakatsuji, H.; Hada, M.; Ehara, M.; Toyota, K.; Fukuda, R.; Hasegawa, J.; Ishida, M.; Nakajima, T.; Honda, Y.; Kitao, O.; Nakai, H.; Klene, M.; Li,

X.; Knox, J. E.; Hratchian, H. P.; Cross, J. B.; Bakken, V.; Adamo, C.; Jaramillo, J.; Gomperts, R. ; Stratmann, R. E. Yazyev, O. ; Austin, A. J. ; Cammi, R. ; Pomelli, C. ; Ochterski, J. W. ; Ayala, P. Y. ; Morokuma, K. ; Voth, G. A. ; Salvador, P. ; Dannenberg, J. J. ; Zakrzewski, V. G. ; Dapprich, S. ; Daniels, A. D. ; Strain, M. C. ; Farkas, O. ; Malick, D. K. ; Rabuck, A. D. ; Raghavachari, K. ; Foresman, J. B. ; Ortiz, J. V. ; Cui, Q. ; Baboul, A. G. ; Clifford, S. ; Cioslowski, J. ; Stefanov, B. B. ; Liu, G. ; Liashenko, A. ; Piskorz, P. ; Komaromi, I. ; Martin, R. L. ; Fox, D. J. ; Keith, T. ; Al-Laham, M. A. ; Peng, C. Y. ; Nanayakkara, A. ; Challacombe, M. ; Gill, P. M. W. ; Johnson, B. ; Chen, W. ; Wong, M. W. ; Gonzalez, C. Pople, J. A. *Gaussian 03, Revision B.03*; Gaussian, Inc.: Wallingford, CT, 2004.

(36) Mulliken, R. S. *J. Chem. Phys.* **1955**, *23*, 1833, 1841, 2338, 2343.

(37) Ehrhardt, C.; Ahlrichs, R. *Theor. Chim. Acta* **1985**, *68*, 231.

(38) Wiberg, K. B. *Tetrahedron* **1968**, *24*, 1083.

(39) Hoffmann, R. *Solids and surfaces: a chemist's view of bonding in extended structures*; VCH Publishers: New York, 1988.

(40) Eyert, V.; Hock, K. H. *Phys. Rev. B* **1998**, *57*, 12727.

(41) Ganduglia-Pirovano, M. V.; Sauer, J. *Phys. Rev. B* **2004**, *70*, 045422.

(42) Wagemaker, M.; Kearley, G. J.; van Well, A. A.; Mutka, H.; Mulder, F. M. *J. Am. Chem. Soc.* **2003**, *125*, 840.

(43) Murnaghan, F. D. *Proc. Natl. Acad. Sci. U.S.A.* **1944**, *30*, 244.

(44) Hermann, K.; Witko, M.; Druzinic, R. *Faraday Discuss.* **1999**, 53.

(45) Loa, I.; Grzechnik, A.; Schwarz, U.; Syassen, K.; Hanfland, M.; Kremer, R. K. *J. Alloys Compd.* **2001**, *317*, 103.

(46) Arlt, T.; Bermejo, M.; Blanco, M. A.; Gerward, L.; Jiang, J. Z.; Olsen, J. S.; Recio, J. M. *Phys. Rev. B* **2000**, *61*, 14414.

(47) Michalak, A.; Witko, M.; Hermann, K. *Surf. Sci.* **1997**, *375*, 385.

(48) Cogan, S. F.; Nguyen, N. M.; Perrotti, S. J.; Rauh, R. D. *J. Appl. Phys.* **1989**, *66*, 1333.

(49) Chakrabarti, A.; Hermann, K.; Druzinic, R.; Witko, M.; Wagner, F.; Petersen, M. *Phys. Rev. B* **1999**, *59*, 10583.

(50) Shin, S.; Suga, S.; Taniguchi, M.; Fujisawa, M.; Kanzaki, H.; Fujimori, A.; Daimon, H.; Ueda, Y.; Kosuge, K.; Kachi, S. *Phys. Rev. B* **1990**, *41*, 4993.

(51) Parker, J. C.; Lam, D. J.; Xu, Y. N.; Ching, W. Y. *Phys. Rev. B* **1990**, *42*, 5289.

(52) Lambrecht, W.; Djafari-Rouhani, B.; Vennik, J. *J. Phys. C: Solid State Phys.* **1981**, *14*, 4785.

(53) Russo, S. P.; Grey, I. E.; Wilson, N. C. *J. Phys. Chem. C* **2008**, *112*, 7653.

(54) Thulin, L.; Guerra, J. *Phys. Rev. B* **2008**, *77*, 195112.

(55) Mo, S. D.; Ching, W. Y. *Phys. Rev. B* **1995**, *51*, 13023.

(56) Asahi, R.; Taga, Y.; Mannstadt, W.; Freeman, A. J. *Phys. Rev. B* **2000**, *61*, 7459.

(57) Wu, Q. H.; Thissen, A.; Jaegermann, W.; Schuz, M.; Schmidt, P. C. *Chem. Phys. Lett.* **2006**, *430*, 309.

(58) Goclon, J.; Grybos, R.; Witko, M.; Hafner, J. *J. Phys.: Condens. Matter* **2009**, *21*, 095008.

(59) Yin, X. L.; Han, H. M.; Endou, A.; Kubo, M.; Teraishi, K.; Chatterjee, A.; Miyamoto, A. *J. Phys. Chem. B* **1999**, *103*, 1263.

(60) Manoilova, O. V.; Podkolzin, S. G.; Tope, B.; Lercher, J.; Stangland, E. E.; Goupil, J. M.; Weckhuysen, B. M. *J. Phys. Chem. B* **2004**, *108*, 15770.

(61) Haber, J.; Witko, M. *J. Catal.* **2003**, *216*, 416.

(62) Calatayud, M.; Minot, C. *J. Phys. Chem. B* **2004**, *108*, 15679.

(63) Goclon, J.; Grybos, R.; Witko, M.; Hafner, J. *Phys. Rev. B* **2009**, *79*, 075439.

(64) Zhanpeisov, N. U.; Bredow, T.; Jug, K. *Catal. Lett.* **1996**, *39*, 111.

JP910685Z